



Parameters Controlling Liquid Plasma Spraying: Solutions, Sols, or Suspensions

P. Fauchais, R. Etchart-Salas, V. Rat, J.F. Coudert, N. Caron, and K. Wittmann-Ténéze

(Submitted April 12, 2007; in revised form July 9, 2007)

This article presents what is our present knowledge in plasma spraying of suspension, sol, and solution in order to achieve finely or nano-structured coatings. First, it describes the different plasma torches used, the way liquid jet is injected, and the different measurements techniques. Then, drops or jet fragmentation is discussed with especially the influence of arc root fluctuations for direct current plasma jets. The heat treatment of drops and droplets is described successively for suspensions, sols, and solutions both in direct current or radio-frequency plasmas, with a special emphasize on the heat treatment, during spraying, of beads and passes deposited. The resulting coating morphologies are commented and finally examples of applications presented: Solid Oxide Fuel Cells, Thermal Barrier coatings, photocatalytic titania, hydroxyapatite, WC-Co, complex oxides or metastable phases, and functional materials coatings.

Keywords ceramic oxide layers, composite materials, influence of spray parameters, reactive spraying, nanostructured materials, plasma spray forming

1. Introduction

Since more than one decade, nanostructured materials are the focus of intensive research. However, up to the end of the nineties, many works have been devoted to the synthesis of different nanomaterials but little work on the consolidation of these nanoparticles (Ref 1). Studies to consolidate these particles have shown that these powders have a strong tendency for rapid grain growth resulting in difficulties to conserve the nanostructure by sintering, hot pressing... However, with the new process of Spark Plasma Sintering (Ref 2), interesting results have shown that high-density nanostructured materials can be reached with a small grain-size. That is why coating technology, especially thermal spraying in general and plasma spraying in particular, combining synthesis and consolidation processes into a single operation can be advantageous to realize nanostructured or at least finely structured materials in one operation (Ref 1). In conventional plasma spraying, solid particles in the size range 10-100 μm produce lamellar structures when lamellae or splats, roughly a few tens to two hundreds micrometers in diameter, with thickness between 1 and 3 μm , are layered. These coatings present numerous defects: micro- and macro-cracks, unmelted particles, pores, poor contact surface area between piled splats (20-50%)... For example, in plasma sprayed

thermal barrier coatings (TBCs), the numerous “planar porosities” (cracks and poor contact between lamellae) contribute to the low thermal conductivity of the plasma sprayed yttria stabilized zirconia (YSZ) but also to the lower spallation life compared to EB-PVD TBCs. That is why, for this application and others, the production of coatings with much smaller splats, with typical sizes between 0.5 and 3 μm , and much less micro cracks than in conventional spraying as well as small porosities (in the 1- μm size range) rather uniformly distributed is very interesting. Unfortunately in conventional spraying, injection of particles below 5 μm in diameter becomes impossible. The velocity, which has to be imparted to them for their penetration within the plasma jet, varies as the reverse of the cube of their diameter, requiring a high carrier gas flow rate (>8-10 slm for argon with an injector 1.8 mm in diameter). Such a cold gas flow rate perturbs drastically the plasma jet and particles “see” it without being accelerated and heated.

A first solution has been proposed, since the mid nineties, by spraying conventional particles 30-90 μm made of agglomerated nanoparticles. The trick consists in finding the narrow spray window where particles will be partially melted, the melted part being “the cement” entrapping unmelted nanograins. Many papers have been published on that; see for example (Ref 3-10). Coating properties, such as hardness, present a bi-modal distribution (Ref 4). The interested reader can see the review paper of Lima and Marple (Ref 10).

The second solution consists in introducing the material to be sprayed as a liquid which can be a solution (saturated or not), a suspension of micro- or nano-sized or sol-gel particles. The pioneers in this field were Karthekeyan et al. (Ref 1, 11) for solutions in dc plasmas and Bouyer et al. (Ref 12) and Gitzhofer et al. (Ref 13) for suspensions in RF plasmas. For both techniques (RF and dc), the first step was the gas-atomization of the liquid. With dc plasmas, where atomization was optimized to achieve droplets in the size range of 1-10 μm , even if authors did

P. Fauchais, R. Etchart-Salas, V. Rat, and J.F. Coudert, SPCTS UMR 6638 CNRS, University of Limoges, Limoges, France; and N. Caron and K. Wittmann-Ténéze, CEA le Ripault, DMAT/SDI/LPTH, Monts, France. Contact e-mail: vincent.rat@unilim.fr.

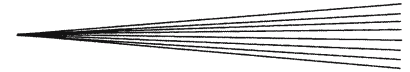
Nomenclature		
Latin Alphabet		
b	Thermal effusivity ($\text{W s}^{0.5}/\text{m}^2 \text{K}$)	ΔP Amplitude of power time fluctuation ($\Delta P = I \times \Delta V$) (kW)
C_D	Plasma drag coefficient (-)	ΔV Amplitude of voltage time fluctuation (V)
d_{dt}	Droplet diameter (m)	κ Plasma thermal conductivity (W/m K)
d_ℓ	Liquid drop diameter (m)	κ_d Pass or deposited layer thermal conductivity (W/m K)
d_i	Internal diameter of injection nozzle (m)	κ_s Substrate or already deposited layers thermal conductivity (W/m K)
d_m	Minimum droplet diameter (m)	ρ Plasma specific mass (kg/m^3)
d_p	Condensed particle diameter (m)	ρ_A Specific mass of atomizing gas (kg/m^3)
f	frequency (Hz)	ρ_ℓ Liquid specific mass (kg/m^3)
h	Heat transfer coefficient ($\text{W}/\text{m}^2 \text{K}$)	σ_ℓ Surface tension of liquid (N/m)
h_p	Plasma enthalpy (MJ/kg)	τ_f Drop or droplet fragmentation time (s)
I	Arc current (A)	$\tau_{v\ell}$ Drop or droplet vaporization time (s)
L_v	Latent heat of vaporization of liquid (J/kg)	
Nu	Nusselt number (-)	
P	Power dissipated in the torch (kW)	
\bar{P}	Time averaged power dissipated ($\bar{V} \times I$) (kW)	
r_ℓ	Drop or droplet radius (m)	
S_i	Surface of injection nozzle (m^2)	
T	Plasma temperature (K)	
T_d	Pass temperature (K or °C)	
T_n	Nucleation temperature (K or °C)	
T_p	Particle temperature (K or °C)	
T_s	Substrate or already deposited layers temperature (K or °C)	
T_M	melting temperature (K or °C)	
U	Velocity difference between plasma and drop or droplet ($U = v - v_\ell$) (m/s)	
U_R	Velocity of atomizing gas relation to that of liquid (m/s)	
v	Plasma velocity (m/s)	
v_ℓ	Injected liquid velocity (m/s)	
v_p	Particle velocity (m/s)	
\bar{V}	Time averaged voltage (V)	
Greek Alphabet		Abbreviations
Δp	Pressure difference between the liquid tank and surrounding atmosphere (Pa)	ALR Atomizing gas/liquid mass ratio (-)
		CCD Charge-Coupled-Device
		CEA Commissariat à l'Énergie Atomique
		dc Direct current
		DTA Differential thermal analysis
		EB PVD Electron beam physical vapor deposition
		HA Hydroxyapatite
		i.d. Internal diameter
		LSCM $\text{La}_{0.75}\text{Sr}_{0.25}\text{Cr}_{0.5}\text{Mn}_{0.5}\text{O}_3$
		RF Radio frequency
		SDC Samarium doped cerium
		slm Standard liter per minute
		SMD Sauter mean diameter (m)
		SOFC Solid oxide fuel cell
		SPCTS «Science des Procédés Céramiques et Traitement de Surface» (Science of ceramic and surface treatment processes), University of Limoges, France
		SPPS Solution precursor plasma spray
		TBC Thermal barrier coating
		TGA Thermo gravimetric analysis
		YSZ Yttrium stabilized zirconia

not mention the phenomenon, the nanostructured coatings obtained with the solution was probably also due to the second fragmentation or atomization of the droplets injected by the high-velocity plasma flow. For conventional plasma torches, with radial injection or with four pilot plasma torches allowing axial injection, spray, feed-stock, and heat treatment parameters strongly influenced the grain size, microstructure, and phase composition of the nano-deposits. For conventional RF plasmas, where velocities are below 100 m/s, no secondary atomization by the plasma occurred. The drops resulting from gas atomization were vaporized, the solid particles contained densified, sintered, and then melted resulting in material drops in the range of tens of micro-meters particles (for example, hydroxyapatite, perovskite, cobalt spinel,...). It

is only recently that, with the development of supersonic nozzles adapted to RF plasma torches, nanostructured dense electrolyte (gadolinium-doped ceria) thin coating were deposited starting from a suspension of this material (initial grain size 20 nm) (Ref 14).

In the following, only nano or finely structured coatings obtained by solutions and suspensions dc plasma spraying will be treated, the results about coatings obtained with supersonic RF being too recent with no written paper to be discussed. The interested reader will find information about:

- Solutions of metal precursor: nitrates, isopropoxides, butoxides... dissolved in water, ethanol, isopropanol... (Ref 15-18),



- Suspensions of micronic or sub-micronic particles (Ref 19-24).

Both processes can deliver fine splats and have the possibility to realize coatings with two or three different materials very deeply intricated (suspensions) or with new chemistry because in solutions the molecular level mixing of constituents allows creating new materials with metastable phases. With suspensions the contact between the solid particles is not necessarily perfect as agglomerates can explode upon solvent evaporation resulting in the separation of components such as zirconia and alumina.

This article will be focused on the liquid spraying either of the solutions or suspensions. In both cases the liquid introduces new problems:

- First, it has to penetrate within the plasma jet and for that the liquid must be atomized or mechanically fragmented. In the following will be called liquid drops those resulting from the production set-up and droplets those resulting of drops fragmentation by the plasma jet.
 - (i) For dc plasma jets especially for radial injection, the momentum density of the liquid drop $\rho_\ell v_\ell^2$, where ρ_ℓ is the specific mass of the liquid drop and v_ℓ the drop velocity, has to be compared to that of the plasma jet ρv^2 , which varies with the plasma jet radial and axial position (i.e., along the drop trajectory). The questions which arise are: Under which conditions drops will be fragmented into droplets by the plasma flow? How fast will droplets vaporize comparatively to drops and how their trajectories will be modified by evaporation? Moreover, dc plasma jets are more or less transient with the arc root fluctuations at the anode (in the 3-8 kHz range), fluctuations which can induce power fluctuations ΔP as high as $\Delta P/\bar{P} > 1$, where \bar{P} is the mean power dissipated within the torch. Such fluctuations have a drastic effect on the plasma jet velocity v (Ref 22) and contribute to the drop dispersion in both the hot and cold zones of the plasma jet.
 - (ii) For RF plasmas with flow velocities below 100 m/s and axial injection the liquid penetration is much easier and requires rather low injection velocities (a few m/s).
- Second, once liquid has penetrated, its vaporization and then dissociation and ionization will cool down the plasma and the phenomena occurring for condensed components contained within the liquid will differ for solutions and suspensions.
- For suspensions with dc jets, the evaporation of the solvent of droplets frees the solid particles they contain. Those traveling in the jet core are accelerated and melted, as in conventional plasma spraying but with the necessity to adjust the plasma conditions to particle sizes to avoid their vaporization. For those traveling in the jet fringes, melting does not necessarily occur.

In conventional RF plasmas, the liquid jet or drops are not fragmented by the flow and vaporization is the dominant process that is much longer than that of fragmented drops. The sub-micronic or micronic particles contained within drops are then flash sintered and melted. The resulting particles are in a molten state and have sizes in the tens of micron range which is similar to that of conventional spraying.

- For solutions depending on droplet size, solvent, percentage of solute, heating rate (trajectory), and properties of dissolved solute, precipitation characteristics can vary significantly and produce very different particle morphologies.
- Third, due to the size of particles impacting the substrate (between 0.1 and few micrometers) and the plasma jet cooling by solvent vaporization, spray distances are usually shorter than in conventional spraying (between 40 and 60 mm with a PTF4 torch for example). It means that the coating under construction is submitted for dc plasma jets to heat fluxes between 6 and 20 MW/m² modifying its structure during spraying, especially for ceramic materials with low thermal conductivity.
- Fourth, according to the complexity of the phenomena involved, modeling is not very easy and, at the moment, only simplified equations can give trends. Diagnostics are also very complex according to the plasma radiation and heat flux as well as sizes of particles formed.

This article will present successively:

- The experimental devices: plasma torches used, liquid injection methods, measurement techniques for particles in-flight and at impact as well as coating characterizations.
- The drops penetration within the plasma jet and their fragmentation into droplets (in dc plasma jets) followed by the vaporization of the solvent with the formation of particles for suspensions and solutions.
- The coating construction for suspensions and solutions.
- Few examples of coatings: TBCs, SOFCs, Photocatalytic titania, hydroxyapatite, WC-Co, metastable phases, and functional materials.

2. Experimental Devices

2.1 Plasma Torches

Practically all types of plasma spray torches have been used for suspension or solution spraying, except to our knowledge, Plazjet and water torches.

2.1.1 Conventional Plasma Torches. Either the PTF4 or the 3MB from Sultz Metco have been used with Ar-H₂, Ar-He, or Ar-He-H₂ mixtures (Ref 15, 17, 19-30). The resulting plasma jets, depending on the anode-nozzle i.d., exhibit temperatures up to 14,000 K at the torch axis and nozzle exit as well as velocities between 1300 and 2200 m/s depending on the gas used, nozzle i.d. (between 6 and 7 mm in general) and arc current (Ref 31, 32). One of

the jet characteristics is its fast cooling down with its expansion in the surrounding atmosphere resulting particularly in a fast decrease of its axial velocity (e.g., from 2000 m/s at the nozzle exit to 1000 m/s 10 mm downstream for $I=622$ A, Ar-45 slm, H_2 -15 slm, anode-nozzle i.d. 7 mm). Of course, this decrease is a little bit less important for lower velocities (from 1000 to 700 m/s in the same conditions but with $I=194$ A).

If one keeps in mind that the momentum density exerted by the plasma jet is ρv^2 , it means that shifting from 2000 to 1000 m/s (e.g., by increasing the torch nozzle i.d.) reduces it by one-fourth even if the slight temperature drop has risen ρ by $<10\%$. It is also important to underline that the radial velocity (Ref 20) decreases also very fast. For example, in the periphery of the jet at 3.0 mm from torch axis and 3 mm downstream of the nozzle exit, the velocity has dropped from 1800 to about 200 m/s, but according to the temperature drop, ρ has been multiplied by about 4.

At last, these conventional torches present very important arc root fluctuations resulting in power fluctuations such as $\Delta P/\bar{P}>1$ for Ar- H_2 or Ar- H_2 -He mixtures and $\Delta P/\bar{P}<0.5$ for Ar-He ones, such fluctuations resulting in strong velocity fluctuations.

2.1.2 Triplex Torches. Their main difference with conventional torches is that they comprise three insulated cathodes supplied by independent sources and distributing the electrical energy to three parallel arcs sticking at a unique anode preceded by insulating rings permitting the generation of long arc of high voltage (Ref 33). The plasma gas is mainly Ar-He. Thus, voltage fluctuations are considerably reduced compared to conventional torches. If the voltage fluctuation is the same as that with a conventional torch working with Ar-He, the mean voltage being about 100 V compared to 40 V, $\Delta V/\bar{V}$ is much smaller. This can be seen by comparing plasma jet pictures taken with a shutter time of 10^{-4} s (Ref 33). The exiting plasma jet shows three areas with highest energy density, arranged in triangular shape (Ref 34). The plasma jets are not very different from those of conventional torches with about the same temperature and probably slightly lower velocities. The liquid injector position has to be optimized relatively to the three high-energy areas (Ref 34). This technique has been used by different authors (Ref 29, 30, 34) for liquid precursors spraying.

2.1.3 Axial Injection. dc Torches. The torch that has mainly been used for solutions and suspensions (Ref 24, 27, 35) is that of Mettech: Axial III (Ref 36). This gun is constituted of three cathodes and three anodes operated by three power supplies (total power ranging from 50 to 150 kW). The three plasma jets converge within an interchangeable plasma nozzle and particles or liquid feedstock are injected axially between the three plasma jets before the converging nozzle. The plasma jet is very little cooled (compared to its expansion in air) by the water cooled nozzle and the material injected is heated first during its travel in the nozzle and then in the plasma jet core exiting the torch which can reach easily 10 cm (without liquid injection). To our knowledge, no measurements have been published on plasma jet velocity and

temperature distributions but a few results obtained with DPV2000 are available about conventional powders injected (Ref 37, 38). For example, with 11-45 μm WC-Co particles and 85 kW with a plasma gas flow rate of 250 slm, velocities reach 400 m/s at 50 mm downstream of the nozzle and 300 m/s at 250 mm with temperatures from 2500 to 2250 °C (Ref 37). With almost the same particles (WC-Co-4Cr) and similar gas flow rates particle velocities were between 300 and 400 m/s at 150 mm with temperatures between 2100 and 2400 °C (Ref 38). This means that the torch is very efficient in momentum and heat transfer with gas velocities probably in the range 1200-2000 m/s at the nozzle exit. As it will be seen in Sect. 6, this torch allows reaching velocities up to 700-800 m/s for zirconia agglomerated nanoparticles with a mean diameter of 5 μm . Another torch with four torches converging to a main anode (Ref 1) has also been used to spray solutions.

RF Torches. RF torches with internal diameters between 35 and 50 mm (Tekna torches) with power levels between 30 and 50 kW have been used to spray mainly suspensions or solutions (Ref 39-44). With such torches, velocities are below 100 m/s and temperatures up to 10,000 K (Ref 45).

RF torches equipped with de Laval nozzle allow spraying particles below 20 μm at velocities up to 1000 m/s. However, these particles are melted before the nozzle throat which requires special injectors to avoid their sticking at the nozzle throat. Very recently, a RF torch equipped with de Laval nozzle has been used to spray a suspension of gadolinium-doped ceria (Ref 46). This torch induces a behavior completely different from that of conventional RF torches, drops being fragmented within the plasma as with dc torches (with axial injection), which induces splats with diameters in the range of 0.5-3 μm .

2.2 Injection Systems

Two main techniques are used: atomization or mechanical injection.

2.2.1 Spray Atomization. It has been used for suspensions and solutions (Ref 1, 11, 30, 47-51). Very often co-axial atomization is used. It consists in injecting a low-velocity liquid inside a nozzle where it is fragmented by a gas (mostly Ar for its mass) expanding within the body of the nozzle (Ref 52). For liquids of viscosity between few tenths to few tens of mPa s, their break-up into drops depends, as it will be seen in details in Sect. 3.2, on the Weber number which is the ratio of the force exerted by the flow on the liquid to the surface tension force. It means that, for a liquid with a given surface tension, atomization depends on gas velocity and specific mass. Atomization also depends, but to lesser extent, on the Ohnesorge number including the effect of liquid viscosity (see, e.g., the study of Rampon et al. (Ref 53)). However, if the viscosity is too high (>0.8 mPa s), feeding troubles appear (Ref 44). Sizes and velocities of drops exiting the injection nozzle are characterized by laser scattering. Measurements show that atomization is affected by the following parameters: the relative velocity liquid-gas, the ratio of the gas to liquid volume feed rates, called RGS (generally

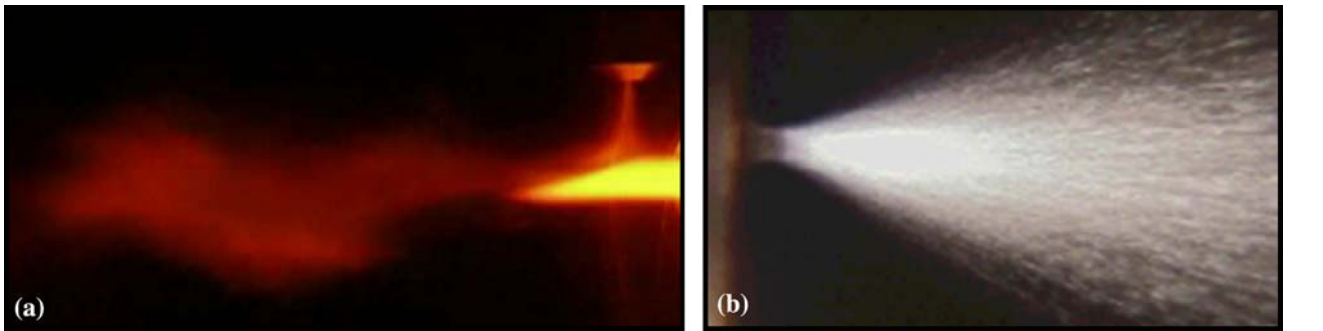


Fig. 1 Interaction of an Ar-H₂ (45-15 slm) dc plasma jet ($I = 600$ A, anode-nozzle i.d. 7 mm) with an atomized ethanol jet (Ref 56). (a) Atomized ethanol jet, (b) interaction plasma-atomized jet

over 100), or the mass ratio between gas and suspension, called ALR (below 1), the nozzle design, the properties of the liquid (density, surface tension, dynamic viscosity) (Ref 52). For example with alcohol, depending on the Ar atomizing flow rate, drops mean sizes vary between 18 and 110 μm (Ref 47). Of course, with the same injection parameters, shifting from ethanol ($\sigma_{\text{eth}} = 22 \times 10^{-3}$ N/m at 293 K) to water ($\sigma_{\text{w}} = 72 \times 10^{-3}$ N/m) modifies the mean diameter from 70 to 200 μm . If increasing the atomizing gas constricts the drops jet, it also perturbs the plasma jet (see Fig. 1). Similar results have been obtained when considering the influence of the ratio of gas flow rate/suspension feed rate (Ref 48), called RGS: the drop size diminishes with the increase of RGS. Quadrupling the RGS leads to a decrease in the drop size by a factor of ten and allows obtaining a narrower Gaussian curve. It is also interesting to note that the weight percentage of solid in the suspension broaden the particle size distribution. For more details see the book of Lefebvre (Ref 54) where it can be found, for example, the relationship existing between the Sauter mean diameter (SMD) and the variables σ_1 , ρ , ρ_l , ALR, μ , and the diameter of the discharge orifice of the atomizing probe. However, at least for suspensions that have a non-Newtonian behavior (generally thixotrope), these expressions, established for Newtonian liquids, must be taken with care.

Similar results about the effect of atomizing gas flow were obtained for solution (Ref 11). Of course, the liquid pressure as well as the atomizing gas mass flow rate and pressure control drop velocities and sizes (Ref 49, 50). Typical sizes obtained are in the range 2-100 μm with velocities varying between 60 and 5 m/s. For example with YSZ solution, the average drop size is 38 μm with an average velocity of 13 m/s (Ref 50). At last it must be underlined that the injector is water cooled in order to bring it as close as possible of the plasma jet to avoid too much dispersion of the drops jet before its penetration within the plasma jet. Very recently, Jordan et al. (Ref 55) have developed a homemade capillary atomizer with a liquid exiting one capillary and an air atomizing jet at 90° to the liquid discharge used as a transverse atomizer. It results in a rather narrow spray jet and drop size distribution in about the 1-20 μm diameter range.

2.2.2 Mechanical Injection. Two main techniques are possible: either to have the liquid in a pressurized reser-

voir from where it is forced through a nozzle of given i.d., or to add to the previous set-up a magnetostrictive rod at the back side of the nozzle which superimposes pressure pulses at variable frequencies (up to a few tens of kHz).

The first device has been developed at the SPCTS in Limoges, France (Ref 19-22, 56-58). It consists of four tanks in which different suspensions and one solvent are stored. Any reservoir or both of them can be connected to an injector consisting of a stainless steel tube with a laser machined nozzle with a calibrated injection hole. A hole of diameter d_i produces a liquid jet with a velocity v_ℓ (m/s) linked to the incompressible liquid mass flow rate \dot{m}_ℓ (kg/s) by:

$$\dot{m}_\ell = \rho_\ell v_\ell S_i \quad (\text{Eq 1})$$

where ρ_ℓ is the liquid specific mass (kg/m^3) and S_i the surface of the nozzle hole (m^2). Assuming that the liquid is non-viscous and ideal, v_ℓ depends on the pressure drop Δp between the tank and surrounding atmosphere through the Bernoulli equation:

$$\Delta p = \frac{1}{2} \rho_\ell v_\ell^2 \quad (\text{Eq 2})$$

However, the right-hand side of this equation has to be multiplied by a correction factor to take into account the friction along the nozzle wall (depending on its shape, length, and roughness) as well as the viscous dissipation. Correction factors between 0.6 and 0.9 are often used. For example, in the experiments performed at Limoges (SPCTS) (Ref 19-22, 57, 58), d_i was 150 μm and tank pressure varied between 0.2 and 0.6 MPa. If, for example, one wants to achieve the same \dot{m}_ℓ as that obtained at 0.5 MPa with $d_i = 150 \mu\text{m}$ with a smaller d_i of 50 μm , it can be deduced from Eq 1 and 2 that p should be multiplied by 81 (a pressure of 40.5 MPa requires adapted equipment and to take precaution!).

The liquid exiting the nozzle, characterized with a CCD camera (diameter and drop velocity), flows as a liquid jet, with a diameter between 1.2 and 1.5 $\times d_i$ depending on the tank pressure and nozzle shape. After a length of about 100-150 $\times d_i$, Rayleigh-Taylor instabilities fragment it in drops, where the size is about 1.3-1.6 \times that of the jet. Thus, depending on the position of the injector exit relatively to the plasma jet (radial injection), it is possible to inject

either the liquid jet or drops. For example, with $d_i = 150 \mu\text{m}$ and a pressure of 0.5 MPa, the drops diameter was $300 \mu\text{m}$ and the flow rate of liquid was $0.47 \text{ cm}^3/\text{s}$. A similar device was used by Siegert et al. (Ref 59) with a nozzle i.d. of $250 \mu\text{m}$.

To overcome the pressure problem, Blazdell and Kuroda (Ref 60) used a continuous ink jet printer which allowed uniformly spaced drops to be produced by superimposing a periodic disturbance on a high-velocity ink stream. They used a nozzle $50 \mu\text{m}$ in i.d. (d_i) and a frequency f operation of 74 MHz producing 64,000 drops/s. Their theoretical diameter d_ℓ was given by Eq 3:

$$d_\ell = \left(\frac{3d_i^2 v_\ell}{2f} \right)^{1/3} \quad (\text{Eq 3})$$

where v_ℓ is the liquid velocity. This expression shows that d_ℓ is a function of the liquid flow velocity and therefore these two parameters cannot be controlled separately. It is also possible to replace v_ℓ by \dot{m}_ℓ using Eq 1.

In their experiments, Blazdell and Kuroda (Ref 60) used a tank pressure of 0.12 MPa corresponding to drops $87 \mu\text{m}$ in mean diameter with a theoretical velocity of 11.5 m/s. According to the nozzle i.d. and the number of drops, the liquid flow rate is about 20× less than in the preceding case (see previous section) where a nozzle $150 \mu\text{m}$ in i.d. was used.

Oberste-Berghaus et al. (Ref 28) have used a similar set-up with a magnetostrictive drive rod (Etrema AU-010, Ames, Iowa) at the backside of the nozzle and working up to 30 kHz. They produce $400 \mu\text{m}$ drops with $10 \mu\text{s}$ delay between each and with a velocity of 20 m/s. Siegert et al. (Ref 29) have used a peristaltic pump with single boring injection, where i.d. is between 0.2 and 0.7 mm, the velocity being varied through the i.d. between 0.7 and 18 m/s.

2.3 Diagnostics

Diagnostics are very complex for the following reasons:

- very bright plasma jet core,
- very fast fragmentation of drops (few microseconds) and vaporization (few microseconds) of resulting droplets,
- size of the condensed phases (few hundreds of nanometers to a few micrometers) contained within droplets, and
- number of particles in condensed phase: 10^8 and 10^{10} part/s. Thus in most cases only indirect means (such as ensemble measurements, pictures taken with laser flash, splat collections...) allow understanding the phenomena.

2.3.1 Drops and Droplets Visualization. The only way to visualize them, relatively to the bright plasma jet, is to use a laser pulse. This has been achieved with the plasma and liquid jets continuously illuminated with a Nd:YAG laser, pictures being taken by a CCD camera (Ref 28). In Limoges (Ref 22), the CCD camera of the Spray Watch[®] system has been used with a fast shutter ($10 \mu\text{s}$) and a filtered diode laser illumination (about $2 \mu\text{s}$ duration) at 808 nm. The laser flash is triggered by the transient voltage signal and pictures can be obtained according to the voltage level of fluctuations (at about 5000 Hz with Ar-H₂ plasma). In the conditions studied, the time required for one drop to travel from the upper edge of the plasma jet down to its axis, 3 mm below, is approximately $100 \mu\text{s}$ when taking into account its velocity, which is about 30 m/s. This time corresponds to the half-period of the arc voltage fluctuations, which is about $200 \mu\text{s}$. At the tip of the injector, the liquid jet is not fragmented, but at about 10 mm downstream, it shows weak instabilities which are amplified when the liquid jet penetrates the plasma jet. Figure 2(a)-(c) gives

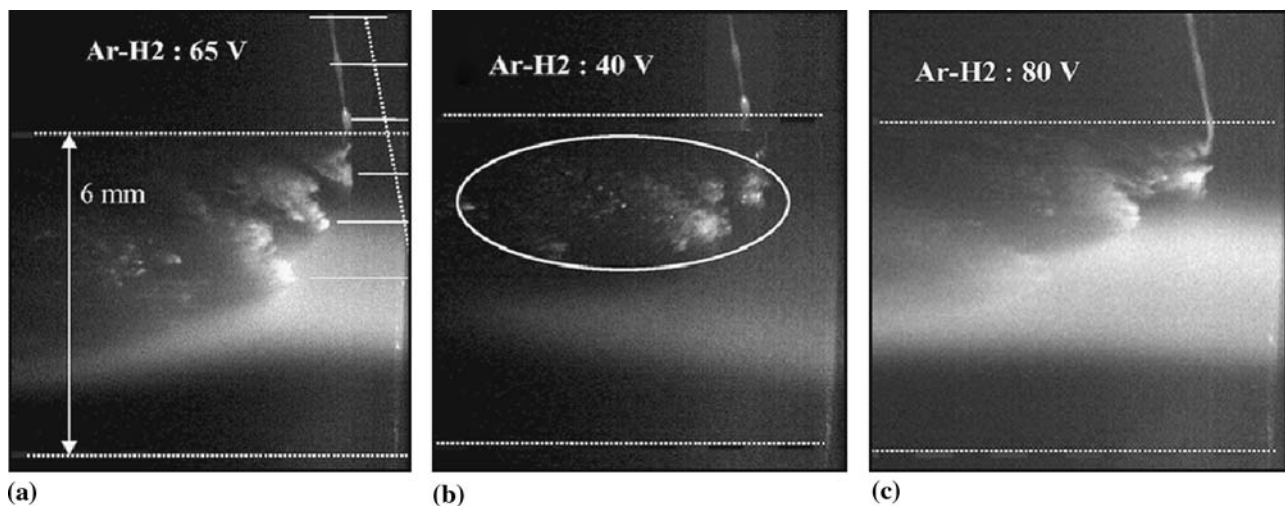


Fig. 2 Plasma-suspension interaction as a function of the triggering level. The feeding pressure (pure mechanical injection) is 0.4 MPa and the suspension volumetric flow rate is $0.47 \text{ cm}^3/\text{s}$. Ar-H₂ 45-15 slm, $I = 500 \text{ A}$, nozzle i.d. 6 mm, transient voltage respectively of (a) 65 V, (b) 40 V, and (c) 80 V



examples of results obtained respectively at 65 V (slightly above mean voltage), 40 V (lowest transient voltage), and 80 V (highest one). The suspension jet is then broken at the neck of the instabilities in the plasma jet and gives individual clouds, or comets, which can be clearly identified in all figures. These comets show a front part, or head, which seems rather compact instead of a sort of tail which develops behind the head and which is composed of tiny drops or dried solid particles. Heads are equally spaced in the direction of injection (tilted line in Fig. 2a) with a 1-mm step corresponding approximately to the wavelength of the jet instabilities before entering the plasma. This means that the velocity is kept in the direction of the injector axis when drops penetrate the plasma. In Fig. 2(a), the first comet, just under the upper edge of the plasma, enters the jet approximately at the time at which the camera and laser are activated, which is also the time at which (within 10 μ s) the arc voltage is 65 V in that particular case.

Instead of that, the third comet, which is close to the axis of the plasma jet in Fig. 2(a), penetrated the jet about 60 μ s before, when the voltage was close to 40 V, as can be deduced from the transient voltage signal. During that time this cloud covered an axial distance of 2 mm and was embedded in a region where the plasma showed a still high-energy density. It can also be seen that the upper parts of the tails are convected at a higher axial velocity than heads, because they are composed of light particles or droplets, much more sensitive to plasma acceleration. An estimation of the particle velocity can be made by considering the fact that all the material belonging to the same cloud enters the plasma at the same time and also the penetration of two consecutive drops is delayed by about 30 μ s.

In the upper part of Fig. 2(b) (40 V), clouds correspond to those collected at the low enthalpy level. No clouds can be observed in the lower part of the figure meaning that drops that have penetrated during the preceding half period have already been swept away. In Fig. 2(c) (80 V), the cloud close to the axis corresponds to that which has penetrated the plasma at the time corresponding to a low level, a few tens of microsecond before. It is interesting to underline the more or less important fragmentation of drops in the plasma jet fringes depending on the transient voltage.

2.3.2 Perturbation of the Plasma Jet by the Liquid Vaporization. Emission spectroscopy, assuming LTE which is more than questionable with liquid injection, can be used to characterize the plasma jet without and with liquid injection. In the latter case, it has been done for Ar-H₂ plasma jets where only water without particles was injected (in the first 2 cm where perturbation occurs, no surrounding oxygen is entrained within the plasma and the only oxygen detectable is that of water injected). Similar results would be obtained when following the injection of ethanol in Ar-H₂ plasma jets. As soon as liquid starts to vaporize, the plasmas are no more symmetrical and new analysis techniques must be used because Abel's inversion is no more possible (Ref 58). Results obtained by Wittmann et al. (Ref 58) show that, as with the suspension, the plasma jet is divided into two parts 5 mm

downstream of the nozzle exit. However, 10 mm farther (i.e., 15 mm downstream of the nozzle exit) the maximum temperature is again located on the plasma jet axis. It means that the water, initially injected, has been completely vaporized, the vapor dissociated in oxygen and hydrogen atoms and ionized, all these elementary species being fully mixed with the plasma, again homogeneous, at that distance. The energy consumed by these processes (before starting heating particles or precipitates) depends strongly on the solvent chosen. For example, only for its vaporization water requires 2.63 MJ/kg against 1.01 MJ/kg for ethanol! Moreover, the combustion of ethanol allows recovering energy, when spraying in air with flames or HVOF. However, it is not necessarily the case in plasma jets because combustion can only occur in regions where temperature is below 3000 K, that is, when spraying in air at distances longer than 70-80 mm downstream the nozzle exit of conventional spray torches, which is not the case with liquid injection.

2.3.3 Particles Collection In-flight. Few attempts have been made to collect solid sub-micrometric particles, after their plasma treatment, by electrophoresis sampling technique. It is based on the attraction of droplets or particles toward an electrostatic precipitator inserted parallel to the stream lines (Ref 11). Another possible mean is to intercept the particles on a substrate disposed at the extremity of a pendulum and traversing the jet at about 1 m/s (Ref 19-21, 56-58) at different distances from the nozzle exit. Of course, the melted particles flatten and form splats while those completely re-solidified or not melted rebound. Similar results can be obtained by moving rapidly (1 m/s) the torch relatively to the substrate positioned at different distances. Of course, to collect such tiny splats the substrate surface has to be polished. Besides, as in conventional plasma spraying (Ref 61), pre-heating the substrate over the transition temperature (see Sect. 5.3) allows obtaining close to disk-shaped splats while on cold substrates splats with irregular shape are collected, as shown in Fig. 3.

It is also possible to collect splats and particles on a substrate protected by a water-cooled shield, disposed at the extremity of an actuator and intercepting particles and plasma fluxes. The substrate is exposed to the particle flux only during a few tenths of seconds. To enlarge the collecting zone of splats and particles in one direction, the line-scan test, as developed by Bianchi et al. (Ref 62) for conventional spraying, can also be used. Similar device has also been used by Siegert et al. (Ref 59). Such systems allow collecting splats and almost spherical particles distributed as shown schematically in Fig. 4.

Particles that have traveled in the hot zones of the jet are well melted and form splats while those that have traveled in the jet fringes form tiny spheres sticking all around the central zone (see Fig. 4).

2.3.4 Velocity and Temperature of Ensemble of Particles. Measuring the velocity and temperature of a single condensed particle in-flight is impossible today because of its mean size (below 1 μ m) but an ensemble measurement can give trends (Ref 24, 27, 28, 35). This has been achieved with a commercial diagnostic system

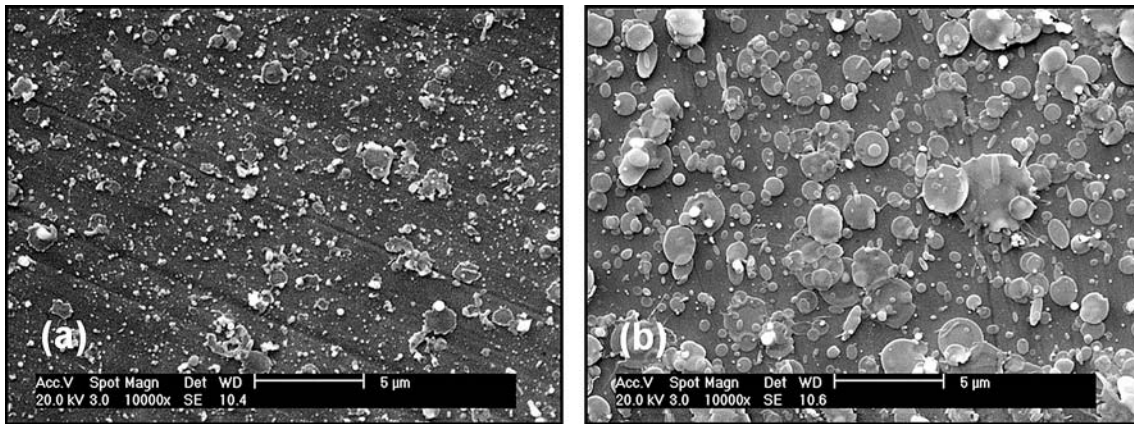


Fig. 3 SEM micrographs of zirconia splats and particles sprayed on 304L stainless steel substrate (a) at room temperature and (b) preheated at 600 K

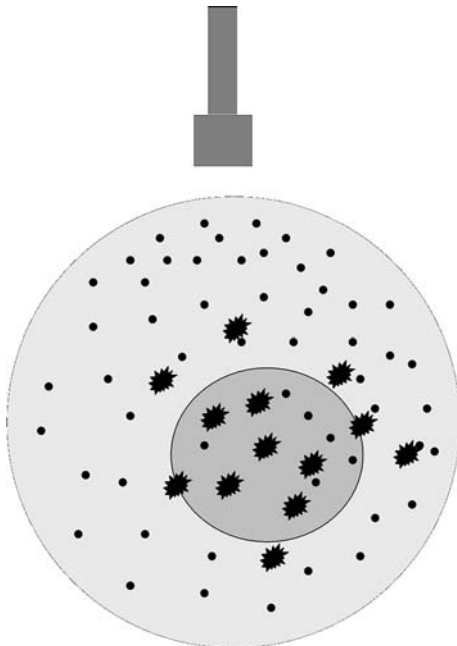


Fig. 4 Schematic distribution of splats and particles collected on a disk-shaped substrate: PT-F4 torch nozzle 6 mm i.d., Ar-H₂ (45-15 slm), $I=500$ A, zirconia suspension 7 wt.%, particle size (0.1-3 μm)

(Accuraspray[®] G2 of Tecknar, St-Bruno, Quebec) acquiring particle emission through two closely spaced optical fibers. The temperature measurement is based on two-color pyrometry, and the velocity is determined by a time-of-flight technique, with cross-correlation calculation (Ref 63). With a conventional spray torch with radial liquid injection the measurement volume is centered in the spray plume, 50 mm downstream of the nozzle exit. The measurement volume is a cylinder 3 mm in diameter and about 25 mm in length, which is orthogonal to the plan defined by the plasma torch and injector axes. With the Mettech torch Axial III, measurements were also achieved between 50 and 62.5 mm downstream of the nozzle exit

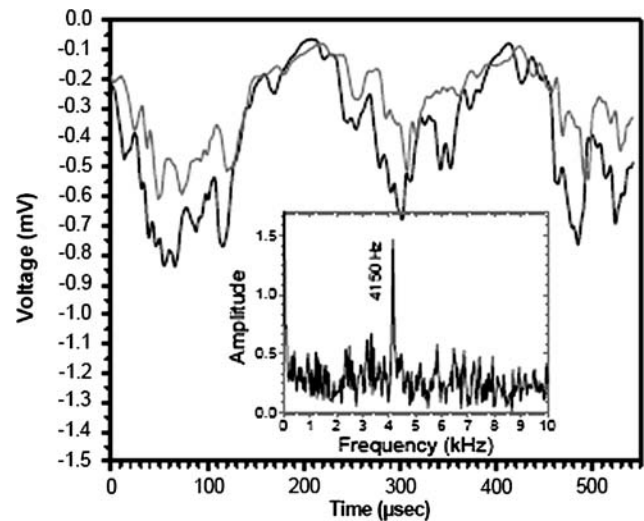


Fig. 5 Accuraspray signal and FFT in an Ar-H₂ plasma produced with a MB-F4 torch in which are injected radially drops of Al₂O₃ suspension with 10 wt.% of powder (particle size: 27-43 μm) (Ref 28)

(Ref 24, 35). A typical signal obtained with a conventional spray torch is shown in Fig. 5. The Fourier transform signal at 4150 Hz coincides with the torch voltage oscillations and Accuraspray signals follow these fluctuations, demonstrating that the small particles follow the gas flow. For example, with the MB-F4 torch working with 600 A, 35 slm Ar, 10 slm H₂ alumina particles mean velocity is 300 m/s while their mean temperature is 2575 °C (Ref 28). With the Mettech torch (Ref 35) working with 200 A (83.2 kW) and 245 slm of Ar (75%), N₂ (10%) and H₂ (15%) and particles of about the same size (29-68 μm), the velocity reaches 574 m/s with a temperature of 2520 °C.

2.3.5 Beads. Another mean to evaluate the degree of melting of particles is to perform line-scan-spray experiments with either a single bead in one passage or overlapped beads with successive passages (Ref 50). The bead thickness depends on the relative velocity torch/substrate,

number of passages, suspension or solution flow rates (or more precisely injection parameters) wt.% of powder or precursors, torch working conditions. What is evaluated is the bead profile, generally assimilated to a Gaussian one, and the adherence of the deposit along the direction orthogonal to the bead. If, in its central part, the bead is mainly constituted of splats embedding unmelted or poorly treated particles, its wings are principally made of piled unmelted or re-solidified particles coming from the jet fringes (see, e.g., Fig. 4) resulting in a powdery deposit. The “wings” of the bead can be partially eliminated by intercepting particles traveling in the jet fringes. This has been achieved with a ceramic plate with a hole 20 mm in diameter in its center and placed in the front of the plasma torch and aligned with its center line (Ref 50) so that the coating material traveling in the plasma jet fringes is shielded from the substrate.

2.3.6 Pass and Coating. As for conventional coatings, cross sections of one or many passes either prepared according to standard metallographic procedures or fractured are studied by optical or scanning electron microscopy (Ref 3, 19, 21, 27, 28). Image analysis is used to determine porosity with or without ultrasonic cleaning after the metallographic preparation to remove or not the unmelted particles. XRD is also performed to determine phases and grain sizes (Ref 27, 28).

2.3.7 Substrate and Coating Surface Temperature. As in conventional spraying, splat formation depends on the substrate temperature (Ref 21, 64), see also Fig. 3, and the residual stress within coating is strongly linked to the mean temperature of coating and substrate as well as temperature gradients within coating (Ref 65). Moreover, as the spray distance is very often much shorter than in conventional spraying (40–60 mm against 100–120 mm for the same PT-F4 torch (Ref 20, 21)), the plasma jet imposes very high heat fluxes which can reach 20 MW/m² at 40 mm for an Ar-H₂ plasma jet (Ref 20). Thus, the temperature measurement of the coating surface is very important and this is achieved by using IR pyrometers (Ref 20, 65), where the response time is generally in the order of 0.1 s. It means that the high-transient temperature induced by the passage of the torch cannot be followed.

2.3.8 Suspensions Preparation. The easiest way is to make simple slurry with particles and solvent, particle sizes varying from a few tens of nanometers to micrometers. The mostly used solvents are ethanol or water or a mixture of both (Ref 23, 47). After stirring, the suspension stability can be tested by sedimentation. Typical values of slurry stability are a few tens of minutes, the stability increasing with the powder load (Ref 48). Slurries with TiO₂, ZrO₂ have been prepared that way (Ref 23, 47, 48, 66) as well as with Al₂O₃ and ZrO₂-Al₂O₃ mixtures (Ref 35). However, nanoparticles of oxides have the tendency to agglomerate or aggregate, even when stirring the suspension.

The stability problem can be overcome by using suitable dispersant, which adsorbs on the particle surface and allows an effective dispersion of particles by electrostatic and/or steric repulsions. The percentage of dispersant must be adjusted in such a way that it displays the minimum

viscosity of the suspension with a shear-thinning behavior (Ref 64). This behavior means that when the shear stress imposed by the plasma flow is low, the suspension viscosity is high and it decreases drastically when the shear stress increases as the drop penetrates more deeply within the plasma flow. For example, with zirconia, a phosphate ester that acts as a combination of electrostatic and steric repulsion has been used (Ref 20). With a mixture of WC-Co (Ref 20), the problem is more complex due to the different acid/base properties of both components: WC or, more precisely, WO₃, at its surface is a Lewis acid, while CoO is basic. Thus, a complex equilibrium between the dispersing agent and the suspension pH must be found; for example, the latter must be adjusted to less basic conditions, but avoiding the cobalt dissolution. Similar problems have been observed with Ni. At last, it must be underlined that when the wt.% of powder increases the viscosity of the suspension increases too. It is also possible to modify the suspension by adding viscous ethylene glycol (where the boiling point is at 200 °C) at the expense of additional thermal load on the plasma (Ref 24). The addition of binders also controls the suspension viscosity almost independently of the dispersion.

It is also important to adapt the size distribution of particles within the suspension to the heat transfer of the plasma jet, limit the width of particles size distribution (as in conventional spraying) in order to reduce the dispersion of trajectories and avoid powders that have the tendency to agglomerate or aggregate, which is often the case of nano-sized particles, especially oxides.

2.3.9 Sol Preparation. A new process called “PRO-SOL” (Ref 67) has recently been developed by the CEA Le Ripault to avoid drawbacks of suspensions with solid particles. It consists in injecting a stabilized suspension of nanometric particles (1–100 nm). This kind of sol-gel solution, called colloidal, is prepared by the hydrolysis and condensation of metallic precursors: the inorganic polymerization reaction (nucleation and growth) is controlled by varying the chemical conditions (pH, hydrolysis ratio...) and allows preparing colloidal particles (1–100-nm particles) directly dispersed in the liquid medium (Ref 68). The method of stabilization permits to avoid the use of additives such as dispersant or add ultrasounds during the deposition phase. Consequently, the main advantages are deposited material purity, very low level of agglomeration and aggregation, well nanostructured coatings featuring sizes below 100 nm, simplification of the process, and the capability of reaching sub-micrometric thickness with high deposition efficiency.

2.3.10 Solution Preparation. Several liquid precursors, such as solution/sol/polymeric complexes, have been evaluated for different oxide systems (Ref 39). The success in forming the phase required for a given system depends on the decomposition characteristics of the different precursors. They include (a) mixture of nitrates in water/ethanol solution, (b) mixtures of nitrates and metal-organics in isopropanol (hybrid sol), (c) mixed citrate/nitrate solution (polymeric complex), and (d) co-precipitation followed by peptization (gel dispersion in water/ethanol). It is important to underline that the molecular

level mixing of constituent chemicals result in chemical homogeneity. It also allows creating metastable coating phases due to rapid cooling of ultra-fine splats during deposition (Ref 49). For example, alumina, YSZ, and zirconia were produced by aluminum isopropoxides, zirconium butoxides, zirconium acetate, and yttrium acetate in isopropanol with *n*-butanol and distilled water as solvents (Ref 11). Other researchers have used aqueous solution of zirconium, yttrium, and aluminum salts (Ref 69-71). According to works related to spray pyrolysis, volumetric precipitation when heating droplets within the plasma jet will probably depend on the solute initial concentration and its value relatively to equilibrium saturation.

3. Drops Fragmentation, Drops, and Droplets Vaporization

In conventional dc plasma spraying, particle penetration within the plasma jet implies that its momentum is close to that imparted to the particle by the momentum density (ρv^2) of the plasma jet. Thus, with a liquid, one has to compare ρv^2 to $\rho_\ell v_\ell^2$ and $\rho_\ell v_\ell^2 > \rho v^2$ results in a good penetration of the drop within the plasma jet. For example, considering an ethanol drop where the injection velocity is 30 m/s, $\rho_\ell v_\ell^2 = 0.7$ MPa, while the plasma flow, assumed to be at 10,000 K with a velocity of 2000 m/s and containing 75% Ar and 25% H₂, has a ρv^2 of about 0.13 MPa. However, upon penetration drops are submitted to a strong shear stress due to the plasma jet, which, under conditions precised later, will fragment them in smaller droplets. Thus, a very important point is the value of the fragmentation time τ_f relatively to the vaporization time τ_v . The fragmentation time can be calculated using simple assumptions (Ref 19). First, it is assumed that atomization is completed when the surface tension force is equal to the drag force of the plasma jet resulting in a minimum droplet diameter d_{\min} such as:

$$d_{\min} = \frac{8\sigma_\ell}{C_D \rho U^2} \quad (\text{Eq 4})$$

where C_D is the plasma drag coefficient and U the velocity difference between plasma and liquid drop. The drag coefficient is that used for plasmas (Ref 72). Using Eq 4 for an Ar-H₂ dc plasma jet, Fauchais et al. (Ref 19) found for pure ethanol $d_{\min} \sim 3$ μm . Of course, it is only an indication because of the steep velocity gradients encountered by the particle along its trajectory. When taking into account the work exerted by the drag force of the plasma jet on the initial drop with a diameter d_ℓ and the surface energy variation to transform one drop of diameter d_ℓ into n droplets of diameter d_{\min} , the fragmentation time can be deduced:

$$\tau_f = \frac{8\sigma_\ell \left(\frac{d_\ell}{d_{\min}} - 1 \right)}{C_D \rho U^3} \quad (\text{Eq 5})$$

When starting with $d_\ell = 300$ μm , with the preceding conditions, it comes $\tau_f \sim 0.15$ μs (Ref 19).

To determine the vaporization time τ_v , one has to calculate the balance between the heat flux imposed by the plasma and that absorbed by the particle when its volume diminishes by vaporization. It results in (Ref 20):

$$\tau_v = \frac{L_v \rho_\ell r_\ell^2}{(T - T_\ell) \kappa Nu} \quad (\text{Eq 6})$$

where L_v is the latent heat of vaporization (J/kg), r_ℓ the liquid drop or droplet radius (m), T the plasma temperature (K) and T_ℓ that of drop (K), κ the thermal conductivity of plasma (W/m K⁻¹), and Nu the Nusselt number (-) corrected to account for the vapor buffer surrounding it (Ref 72).

With 300 μm drop and conditions used for its fragmentation, its vaporization would require 500 μs (to be compared with the 0.15 μs for its fragmentation). Thus, in the following, it can be assumed that fragmentation occurs first. Of course, once fragmented, droplets evaporate much faster than drops: for example, in the previous conditions with $d_{\min} = 3$ μm , vaporization takes place in about 1.5 μs against 500 μs for a drop of 300 μm . These results explain what happens to the Ar-H₂ plasma jet upon water drop penetration (Ref 58). The plasma jet is cut into two parts distributed on both sides of the plan defined by the torch and the injector axis, but the axial symmetry is recovered 15 mm downstream of the nozzle exit, confirming that once droplets are vaporized the solvent vapor is transformed into plasma rather fast.

With the Ar-H₂ plasma described in (Ref 58), droplets velocities a few millimeter downstream of the injector and measured by taking pictures with laser flash are in the 100 m/s range. The time required for traveling the 15 mm is thus about 100 μs , time quite sufficient for complete vaporization of droplets (a few microseconds) and then liquid dissociation and ionization.

3.1 More Elaborated Descriptions of Fragmentation

The study of Hwang et al. (Ref 73) about fuel drops 189 μm in diameter injected at 16 m/s and fragmented by an air jet with velocities between 70 and 200 m/s at 450 K correspond to typical sizes used in plasma with similar gas momentum densities. The different mechanisms depend strongly on the Weber number:

$$We = \frac{\rho \Delta U^2 d_\ell}{\sigma_\ell} \quad (\text{Eq 7})$$

and the different regimes for break-up are defined in (Ref 74). For practical purposes, $We \sim 14$ has been chosen as the critical value over which particles break up (Ref 75). Other authors propose $We \sim 12$. The former value is the criteria adopted by Ozturk et al. (Ref 76, 77) and Basu et al. (Ref 78); with Ar-H₂ and Ar-He conventional dc plasma jets, in the jet core and its fringes ($T > 3000$ K), ρv^2 values are between 15 and 120 kPa. Thus, ethanol droplets down to 15 μm can be broken up in the jet fringes, but when penetrating the plasma up to regions where $\rho v^2 = 50$ kPa, 4 μm droplets will be broken up. This, in

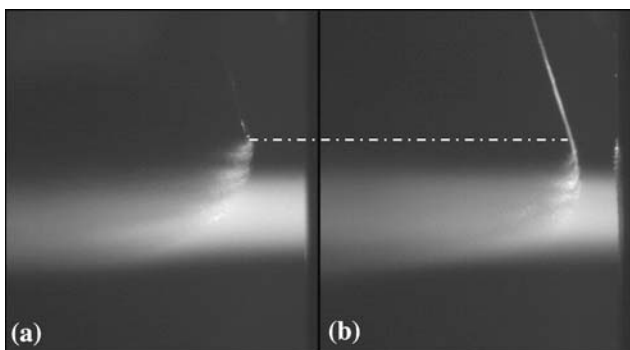


Fig. 6 Influence of the liquid jet composition upon its break-up by Ar-H₂ dc plasma jet. (a) Pure ethanol and (b) zirconia suspension. Exposure time 50 μ s, five laser flashes of 1 μ s duration with 5 μ s between each

good agreement with the simplified calculations presented in Sect. 3.1, particle fragmentation will be more the rule than the exception. Of course, increasing σ_ℓ , for example, by replacing ethanol by water modifies the minimum size of drop break-up which is multiplied by a factor 3.27 (ratio of the surface tensions) and thus small drops (below 40–50 μ m) will be mainly fragmented deeper in the plasma jet and not in its fringes. This is illustrated in Fig. 6 representing the penetration of mechanically injected pure ethanol and the corresponding suspension with 7 wt.% zirconia particles. The addition of solid particles and dispersant enforces the cohesion of the droplet. The fragmentation of the ethanol (left) starts before that of suspension (right), the white dotted line corresponding to the nozzle diameter.

To determine particle trajectories, the momentum equations, in the torch axial and radial directions, as used when spraying micrometric particles, are utilized (Ref 79). Along the trajectory, when they penetrate within the plasma jet, their break-up can be calculated by simple expressions such as those from which Eq 4 is derived. More sophisticated model such the Taylor Analogy Break-up model (Ref 80) can be used (see Basu et al. (Ref 78)). The new trajectory of droplets is again calculated through the momentum equations, taking into account their vaporization. In Eq 4 and 7, the surface tension σ_ℓ of drops and droplets plays a key role. It diminishes with liquid heating:

$$\sigma_\ell = \sigma_\ell^0 - aT \quad (\text{Eq 8})$$

and in principle, the drop or droplet heating along its trajectory should be calculated to account for σ_ℓ modification. However, taking into account the considerations of Sect. 3.1, vaporization is a very slow process compared to fragmentation and drop heating can be calculated on the basis of lumped capacity model.

3.2 Influence of Arc Root Fluctuations

The voltage fluctuations (in the restrike mode with a PTF4 torch and an Ar-H₂ mixture) correspond to a voltage varying between 40 and 80 V for the same arc current of 503 A. The torch velocity follows the

corresponding enthalpy variations while the temperature is almost constant (<1000 K difference when the enthalpy is doubled) due to the “inertia wheel” effect of ionization. Thus, the momentum density of the plasma varies drastically, especially in the jet fringes. The transient momentum density values have been calculated by Marchand et al. (Ref 81). They have used a three-dimensional (3D) and time-dependent model of the plasma jet issuing in air in conjunction with a Large Eddy Simulation (LES) turbulence model to examine the influence of the arc voltage fluctuation amplitude and frequency on the time evolution of the plasma jet flow fields and drops injection. Typical results of the values of the momentum density of the plasma, ρv^2 , in a plan orthogonal to the jet axis and located at 8 mm from the nozzle exit, are presented in Fig. 7. These results were obtained for an Ar-H₂ plasma jet at 600 A. T being the period of the restrike mode, Fig. 7 represents five images of ρv^2 calculated at times differing by $T/5$; in this figure the isotherm 8000 K has been represented in white. This figure shows that the momentum density varies drastically with time for the same position as well as the position of the hot zone of the plasma (8000 K isotherm). As already emphasized, this is due to the variation in length of the electric arc and location of the anodic arc root. Such calculations well underline the very inhomogenous dynamic treatment that drops could undergo (see Fig. 2).

To get more information from images as those presented in Fig. 2, up to 10 images have been superposed and their treatment has allowed determining their envelop and thus measuring the liquid droplets dispersion angle θ and mean deviation α , as shown in Fig. 8. Of course, the results obtained depend on the torch voltage level as illustrated in Fig. 9 for zirconia suspension in ethanol. It can be readily seen that the deviation angle is not very sensitive to the voltage fluctuation (58° at 40 V against 60.5° at 80 V). It is not the case of the dispersion angle which varies from 33° at 80 V against 64° at 40 V. Of course, the deviation angle increases with the injection velocity v_1 . For 300 μ m drops, v_1 varied from 26.6 m/s ($\rho_\ell v_\ell^2 = 0.61$ MPa) to 33.5 m/s ($\rho_\ell v_\ell^2 = 0.96$ MPa) and measurements performed for the lowest transient voltage (see Fig. 10). The dispersion cone becomes narrower and closer to the jet axis when v_1 increases, which also means that fragmentation is more efficient and occurs less in the jet fringes.

Similar results were obtained, as illustrated in Fig. 11, with Ar-He (30-30 slm) plasma jets obtained at 700 A with PTF4 torch where the anode nozzle i.d. was 6 mm. It can be seen that with a rather low voltage fluctuation in the takeover mode ($\Delta V = 10$ V for a mean voltage of 42.4 V) compared to Ar-H₂ ($\Delta V = 10$ V for a mean voltage of 60 V), the dispersion cone is much lower: 15°, against more than 60° for Ar-H₂, the fragmentation also occurs closer to the torch axis and less drops are fragmented in the jet fringes. Measurement of collected particles and splats, as those presented in Fig. 4, show that, with Ar-He, provided the particles sizes of the suspension are adapted, much less particles that have not formed splats are observed.

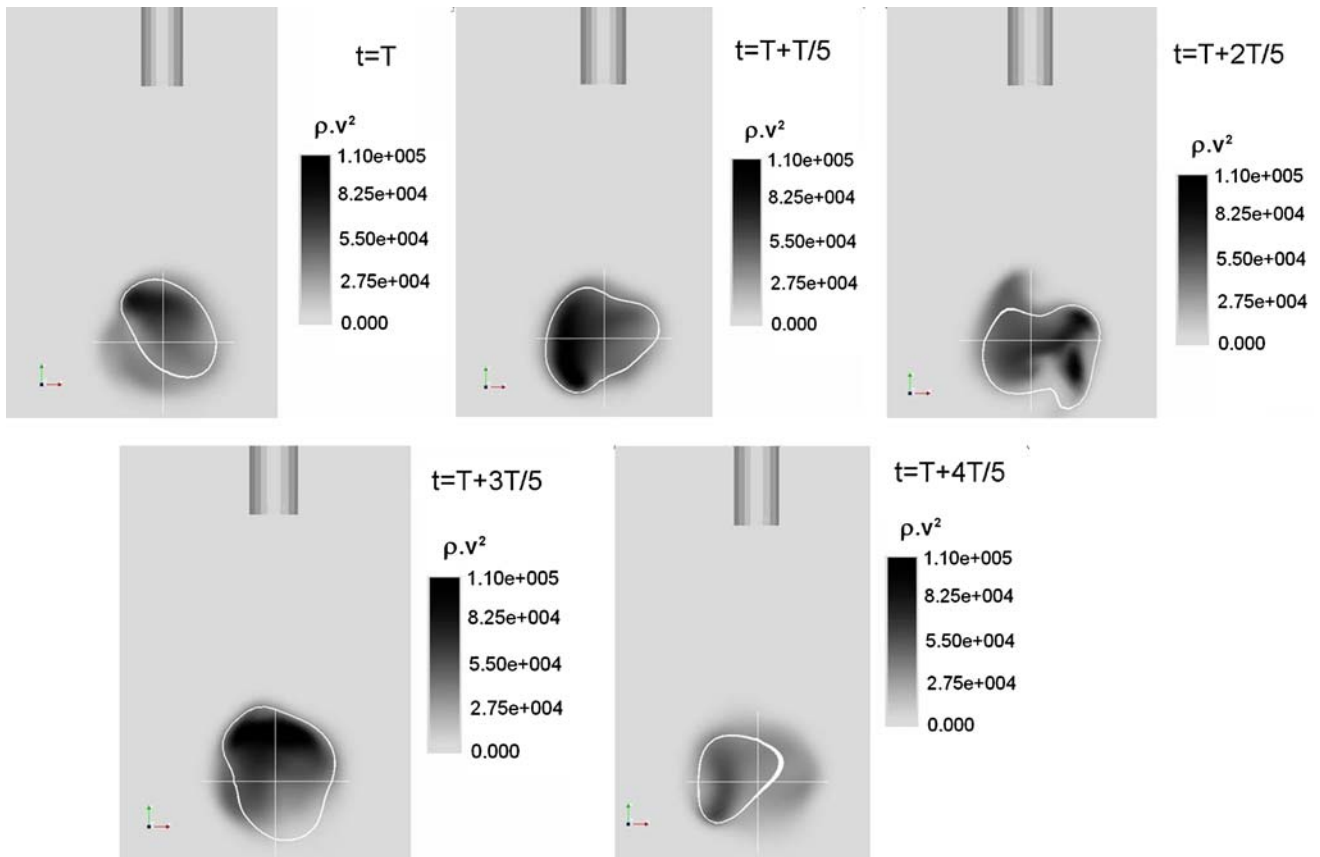


Fig. 7 Calculated momentum density (Pa) of a dc plasma jet in an orthogonal plane to the jet axis at 8 mm from the nozzle. Ar-H₂ (45-15 slm), $I=600$ A (Ref 81)

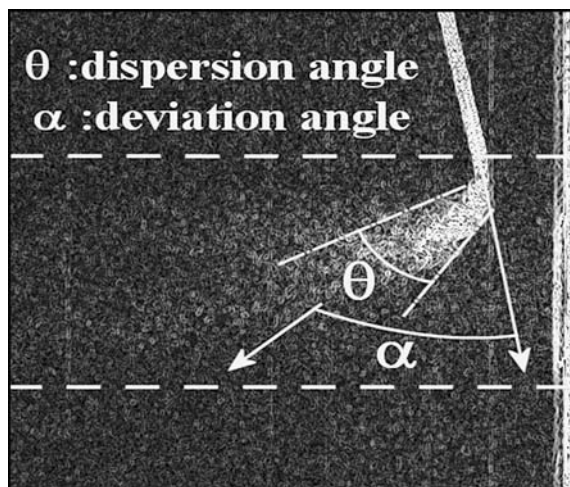


Fig. 8 Definition of the dispersion angle θ and deviation angle α of the liquid droplets cloud (Ar-H₂ dc plasma jet)

3.3 Conclusions

Fragmentation of drops by the plasma jet plays a key role in their further heat treatment. This is due first to the vaporization time of the solvent which varies as the square of the drop diameter and second to droplet trajectories in

the plasma jet core or in its fringes. Based on $We \geq 14$, fragmentation will never occur in RF torches according to the very low plasma velocity ($v < 100$ m/s) for drops injected with sizes between 30 and 280 μm . Thus, all phenomena will be governed by particle heating, solvent vaporization, which are long processes requiring times between a few tens and few hundreds of microseconds depending on particle size distribution.

With dc plasma jets, both in radial and axial injection, particles will be broken up depending on their size and surface tension. The latter can be controlled by using different solvents: ethanol, water, their mixture... by adding to them dispersants, glycol... or increasing the solid particles or precursors load. Diminishing the size and/or increasing the surface tension in radial injection reduce the quantity of drops fragmented, then dispersed and heated in the jet fringes.

4. Heat Treatments Under Plasma Conditions

In this section, the heat treatments of drops or jets of suspensions and solutions as well as successive passes will be successively discussed.

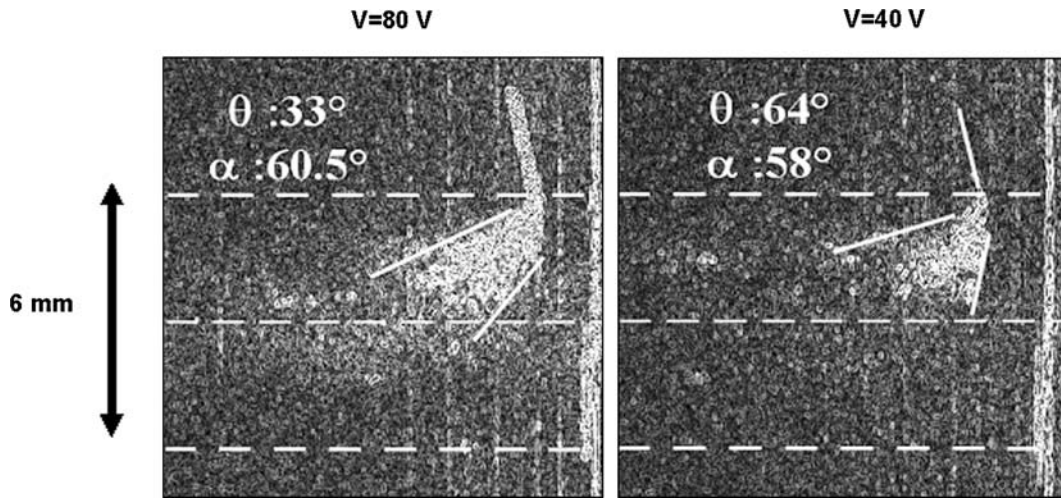
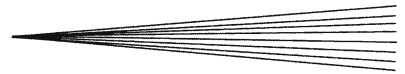


Fig. 9 Evolutions of the dispersion angle θ and deviation angle α of the liquid droplets cloud (Ar-H₂ dc plasma jet) for two transient voltages corresponding to their minimum (40 V) and maximum (80 V) values

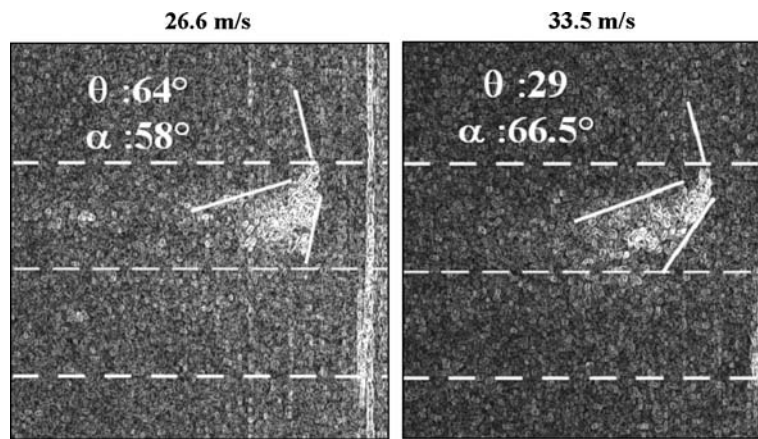


Fig. 10 Evolutions of the dispersion angle θ and deviation angle α of the liquid droplets cloud (Ar-H₂ dc plasma jet) for two drop injection velocities: 26.6 and 33.5 m/s with the transient voltage at its minimum of 40 V

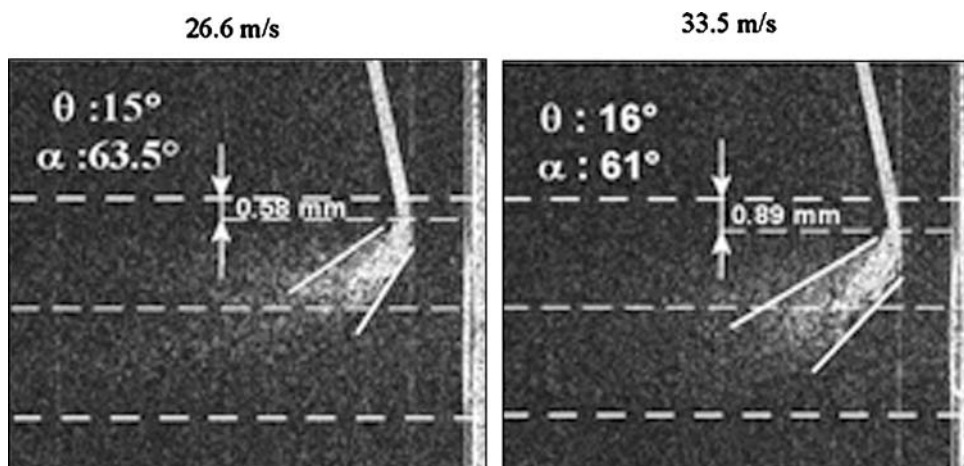


Fig. 11 Evolutions of the dispersion angle θ and deviation angle α of the liquid droplets cloud (Ar-He dc plasma jet with a very low voltage fluctuation level)

4.1 dc Plasma Jets

4.1.1 Suspensions.

Droplets. Once droplets have reached their minimum size, d_m , the solvent is vaporized. The particle vaporization is calculated with the help of the energy balance equations (Ref 74):

$$\frac{d(d_m)}{dt} = -\frac{Q}{\pi d^2 \rho_h L_v} \quad (\text{Eq 9})$$

where Q is the plasma heat transferred by conduction-convection:

$$Q = \frac{\pi d_m^2}{4} h(T - T_c) \quad (\text{Eq 10})$$

The plasma heat transfer coefficient h ($\text{W}/\text{m}^2 \text{K}$) is calculated with the help of Nusselt number, of course modified to account for temperature gradients within the boundary layer surrounding the droplet, the Knudsen effect, and the vapor thermal buffer (Ref 79). In these equations, it has been assumed that droplet temperature is constant (no heat propagation). Equations 9 and 10 show that the plasma temperature must be calculated along the droplet trajectory, which varies as the droplet radius diminishes with its vaporization. It implies a coupling between energy and momentum equations to readjust continuously the particles trajectory. Fragmentation of drops by dc plasma jets plays a key role in the droplets heat treatment, the vaporization varying as the square of particle diameters. If higher surface tension favors the reduction of fragmentation in the jet fringes, for example by using water instead of ethanol, the specific heat and latent heat of vaporization are larger with the former. Under the same conditions, a 2.5- μm water droplet will vaporize in 0.21 μs against 0.13 μs for ethanol. Water as solvent, which increases the surface tension of drops, reduces, after droplets vaporization and transformation into plasma, the energy available to melt suspension particles. This is illustrated in Fig. 12 for a suspension of zirconia particles (Tosoh powder) made with either water or ethanol and sprayed with an Ar-H₂ plasma where the arc current was limited to 300 A to reduce the energy of

the plasma (Ref 82). In such conditions, particles contained in ethanol are melted while those in water are very poorly melted. Once the solvent is completely evaporated (which occurs along trajectories of about 10-15 mm with the radial injection in conventional plasma torches), the treatment of particles contained within droplet will depend on their size distribution and morphology (Ref 21, 83).

Solid particles

Particles traveling in the hot zone of the plasma. Results will be drastically different depending on the ability of solid particles contained in the liquid to agglomerate, or worst to aggregate. Particles (yttria stabilized zirconia) made by attrition milling, after the solvent evaporation, are accelerated (their initial velocities being those gained by droplets before their complete vaporization), heated, and melted by the plasma as schemed in Fig. 13. Of course, the plasma gas composition and enthalpy have to be adapted to particle size distribution and it must be kept in mind that plasma-particle heat and mass transfers are seriously reduced, especially by Knudsen effect. For example, with a mean Ar-H₂ plasma jet temperature of 11,000 K, the correction coefficient for the Nusselt coefficient is 0.013 for 1 μm particles at 2000 K and 0.0013 for 0.1 μm particles at the same temperature. In this case the splat distribution follows rather well the particle size distribution with a flattening degree of about 2 (Ref 21, 83). However, due to the good heat transfer of hydrogen, particles below 0.4 μm are either vaporized and afterwards re-condensed or, for those only melted in-flight, re-solidified at the spray distance. This is illustrated in Fig. 14 showing splats and tiny spherical particles collected 4 cm downstream of the nozzle exit with a stainless steel substrate traversing the plasma jet at 1 m/s at the extremity of a pendulum.

When using nanosized particles obtained by a chemical process (commercial YSZ Tosoh[®] powder), where the size distribution is between 0.1 and 3 μm , due to the agglomeration and aggregation of the initial grains (mean size of 25 nm), the behavior upon solvent vaporization is different. It seems that the bigger agglomerates or aggregates explode upon solvent evaporation resulting in molten

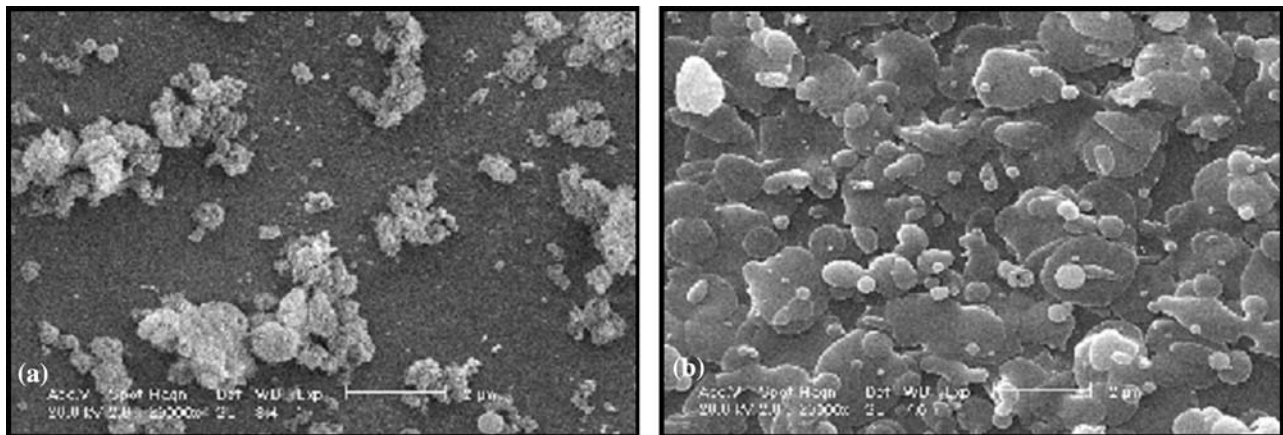


Fig. 12 Influence of the solvent used: (a) water and (b) ethanol; spray conditions: Ar-H₂ (45-15) nozzle i.d. 5 mm, $I = 300$ A

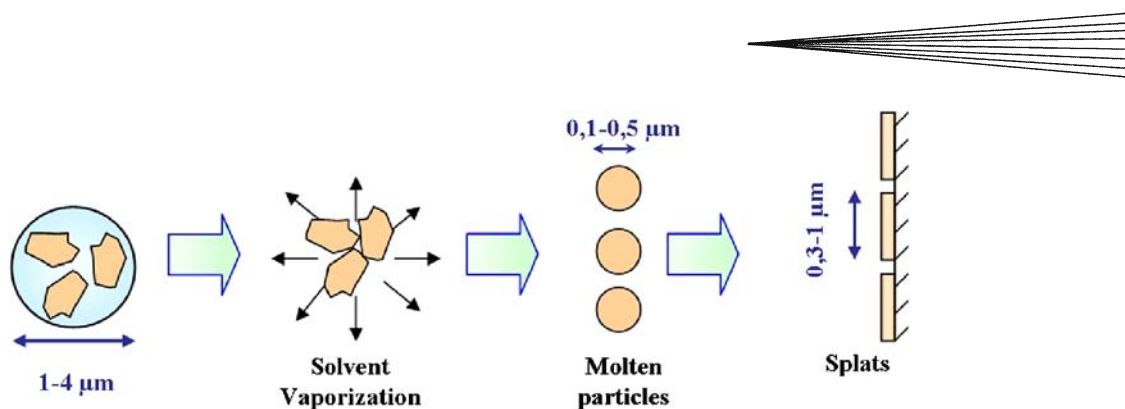


Fig. 13 Scheme of suspension droplet treatment when containing attrition-milled particles

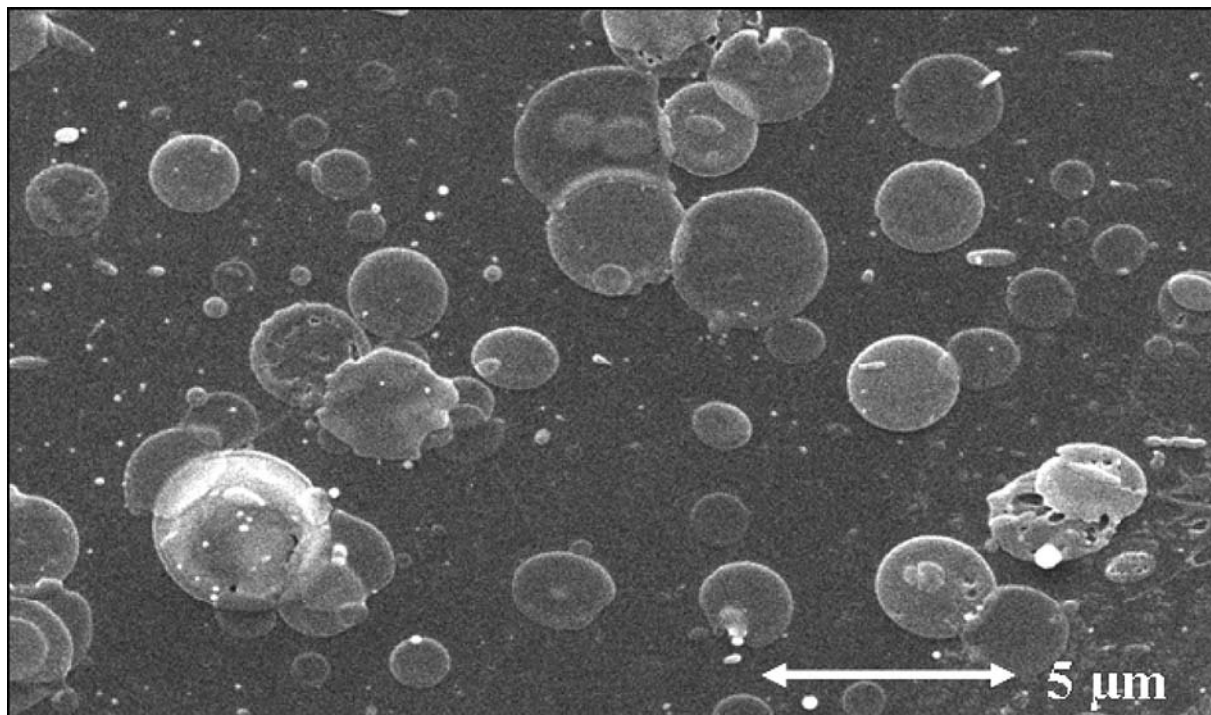


Fig. 14 Splats and particles (re-condensed or re-solidified) collected at 40 mm downstream of the nozzle exit with a smooth stainless steel substrate when spraying attrition milled YSZ particles (between 0.1 and 3 μm) with an Ar-H₂ (45-15 slm) plasma jet, $h_p = 17.9$ MJ/kg

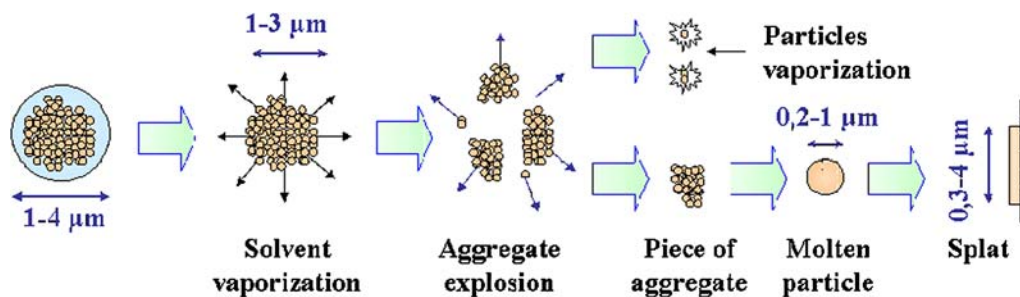


Fig. 15 Scheme of the suspension droplet treatment in the plasma jet for the Tosoh[®] nanometric powder containing aggregates and agglomerates resulting in a size distribution between 0.1 and 3 μm

particles, and smaller particles evaporation as illustrated in Fig. 15. Of course, in this figure the aggregates, which have not been melted and have rebounded on the

substrate, are not represented. Here again most splats are between 0.3 and 3 μm, as illustrated in Fig. 16, showing that they mainly result from agglomerated particles below

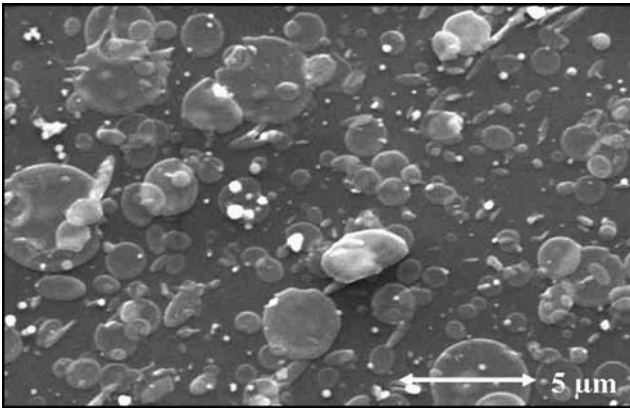


Fig. 16 Splats and particle collected at 40 mm downstream of the nozzle exit with a smooth stainless steel substrate when spraying Tosoh® nanometric particles (between 0.1 and 3 μm) with an Ar-H₂ (45-15 slm) plasma jet, $h_p = 17.9$ MJ/kg

1-2 μm. Besides splats and tiny particles, particles with elongated shape can be observed for which no clear explanation has been found yet.

Particles traveling in the colder zone of the plasma jet. In this case mostly tiny spherical particles (below 0.3 μm) are collected, corresponding to fused and re-solidified or evaporated and re-condensed tiny particles, the untreated particles probably rebounding.

Particle impact. Results presented above indicate particles with sizes down to 0.3 μm impacting the substrate to form splats as well as particles as small as about 0.1 μm sticking on it. The question which is raised and has been underlined by Jordan et al. (Ref 84) is the following: How such small particles will reach the substrate without turning with the gas flow according to their low inertia? The answer relies on the Stokes number:

$$St = \frac{\rho_p d_p^2 v_p}{\mu_g \ell_{BL}} \quad (\text{Eq 11})$$

where the index p is related to the condensed particle, g to the gas, and ℓ_{BL} is the fluid boundary layer thickness. St must be larger than 1 for the particle to reach the substrate. Considering a zirconia particle with an impact velocity of 300 m/s, a boundary layer of 1 mm and an Ar-H₂ plasma containing 30% air (50 mm spray distance) it comes $St \approx 10$ for a 1-μm particle and $St = 1$ for a 0.3-μm particle. It thus means that such sizes are the limit which depends strongly on particle impact velocities. As already indicated in Sect. 2.3.4 in conventional spraying for zirconia particles with a mean diameter of 30 μm, particle velocities up to 300 m/s have been measured with a PTF4 torch against 574 m/s with the Mettech Axial III torch, which permits spraying smaller nanoparticles.

4.1.2 Sol. Stable sols of zirconia nanoparticles in water have been synthesized starting from zirconium and yttrium chlorides with water and urea (CEA patent) (Ref 68). This zirconia sol charged at 10 wt.% has been sprayed with a dc Ar-H₂ plasma jet. In this sol, two zirconia phases are present: monoclinic and quadratic. Traditionally in

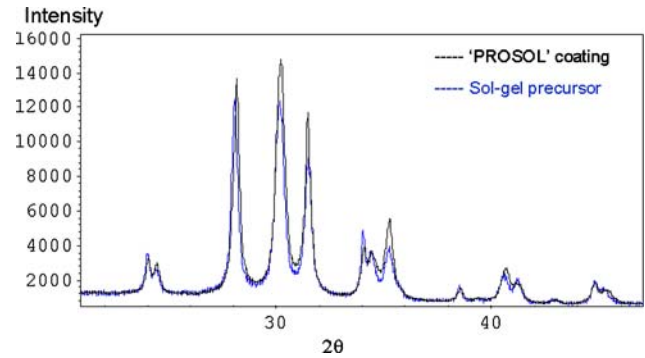


Fig. 17 XRD patterns of sol precursor and resulting plasma sprayed coating (Ref 68)

plasma spraying, the plasma-sprayed zirconia phase is quadratic with a weak quantity of monoclinic phase due to unmelted particles or partially melted ones, whatever the initial phase. In the PROSOL process (Ref 68), the structure and the proportion of the crystalline phases through the coating are typically the same as those of the injected sol as shown in Fig. 17. In the coating, the crystallite size range is between 10 and 20 nm, which is nearly equivalent to the mean diameter of the injected ones equal to 9 nm, as shown in Fig. 18.

4.1.3 Solutions. As described by the model of Ozturk and Cetegen (Ref 85) and Basu et al. (Ref 78), besides the momentum and heat transfer equations between drops or droplets and plasma, the conservation of solute mass and energy equation have to be considered. As for the suspension drops, solution ones are first fragmented, the droplets heating precipitating the solute as a shell. Then, compared to the suspension droplets, where the diameter is controlled by the solvent evaporation, the solution droplet size is now fixed by the outer diameter of the precipitate shell formed under droplets heating. The interior of the droplet is divided into three zones: solid shell, liquid core, and vapor annular between them. Depending on the solute and solvent characteristics and thermo-physical conditions controlling the precipitation, the shell will be more or less porous. The pressure of the vapor inside it, depending on the rate of vapor leaving it, that is, the shell porosity, can be calculated as well as the critical pressure over which the shell will fracture (if its failure stress is known). The precipitate formation depends on droplet sizes and solute initial mass fraction. In small droplets (5 μm in diameter), precipitation, whatever may be the initial solute level, encompass the whole droplet, thus creating solid particles (Ref 78). For larger particles (only particles up to 40 μm were modeled) shell precipitate is formed and fragments, depending on the vapor pressure within particle. Thus, the drops fragmentation and resulting droplets penetration within the plasma jet core or its fringes again play a key role as underlined by Jordan et al. (Ref 84) and Gell et al. (Ref 49). Figure 19 from (Ref 49) illustrates the different mechanisms including precursor solute precipitation, pyrolysis, sintering, melting, and crystallization.

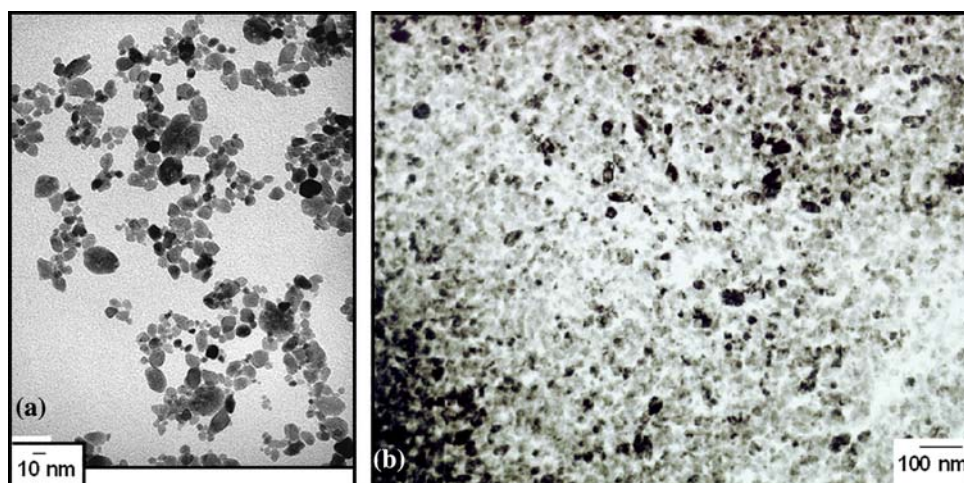


Fig. 18 TEM observation of (a) zirconia sol and (b) resulting coating (Ref 68)

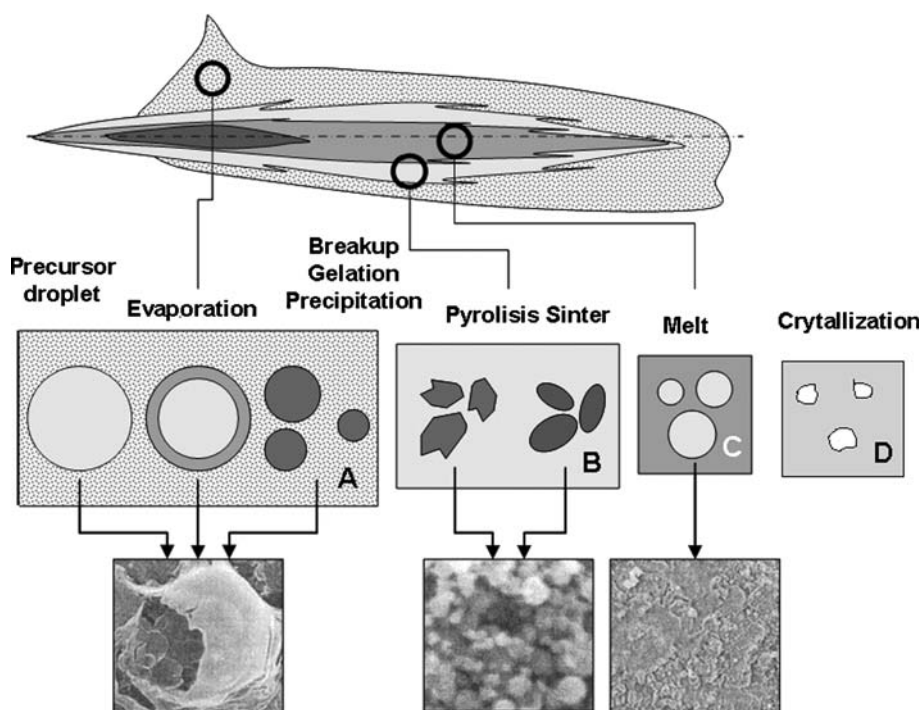


Fig. 19 Schematic illustration of the different treatments of solution droplets within a dc plasma jet (Ref 45)

According to Gell et al. (Ref 49) and Jordan et al. (Ref 84), particles traveling in the hot core of the plasma jet exhibit mechanisms A, B, and C of Fig. 19. If the stand-off distance increases molten particles may re-solidify and crystallize before impact (D mechanism). When droplets travel in the jet fringes but still in the hot area ($T < 4000\text{--}5000\text{ K}$), A and B (Fig. 19) mechanisms are the most probable. At last for droplets traveling in the low temperature regions of the jet, some precursor solution can reach the substrate in liquid form.

With the new injector developed (Ref 55) (see Sect. 2.2.1), it is now possible to avoid most of drops fragmentation in the

jet fringes and drops are mainly treated in the plasma jet hot core. It results in zirconia (YSZ) coatings almost fully dense (more than 97%) (Ref 55).

4.2 RF Plasma Spraying

4.2.1 Suspensions. In this case no fragmentation occurs and the drop solvent evaporation is the main mechanism. In most cases drops are introduced by gas atomization (Ref 39-44, 51) with a mean diameter of few tens of micrometers (up to $90\ \mu\text{m}$). The main phenomenon for suspension is the solvent evaporation followed by flash

sintering and, depending on the plasma conditions, initial drop sizes, load melting, and even evaporation. Collected particles are either fully devoted to materials which are prone to decomposition such as hydroxyapatite, perovskite, photo-catalytic active titania, cobalt spinel, AlN-iMo... and a compromise has to be found between drop treatment (solvent evaporation, sintering...) and material decomposition.

Using a suspension (glycerin-nitrate) of gadolinium-doped ceria (d_{50} of powder ~ 20 nm) and a supersonic RF plasma coating, formed of solidified splats in the range 0.5–3 μm , were achieved (Ref 46). According to authors they were very dense with a gas permeability of zero!

4.2.2 Solutions. Besides suspensions, solution is also used with RF torches (Ref 39). Several liquid precursors—solution, sol, and polymeric complexes—have been tested (Ref 39) for different oxide systems. The possibilities are rather wide (Ref 39) with: mixtures of nitrate in water or ethanol (solution), mixtures of nitrates and metal organics in isopropanol (hybrid sol), mixed citrate-nitrate solution (polymeric complex), and co-precipitation followed by peptization (gel dispersion in water or ethanol). Results strongly depend on the decomposition characteristics of the precursor. This technique allows depositing complex materials such as Yttrium Aluminum Garnet, Yttrium Iron Garnet... synthesized during the plasma treatment and coatings can be dense and nanostructured.

4.3 Coating Heating by the Plasma Jet during Spraying

With dc plasma jets, according to the size of sprayed particles (below 5 μm) and their very low inertia, spray distances are much shorter than in conventional spraying (between 40 and 70 mm against 100–120 mm). In RF plasma, spraying is performed in controlled atmosphere chamber and in most cases coatings are not cooled, except through the substrate, which is not an efficient mean when spraying ceramic coatings with low thermal conductivity. It means that, with RF or dc torches, the coating heating during its formation will play a key role in its structure morphology. It will be illustrated through two examples with zirconia coatings obtained by suspension and solution spraying with a dc conventional torch.

4.3.1 Suspension Plasma Spraying of Zirconia. When spraying with a dc conventional plasma torch, heat fluxes depending on the plasma forming gas, torch working conditions, and spray distance are between 6 and 21 MW/m^2 (Ref 21). For example, with zirconia suspension sprayed on a stainless steel substrate, each pass is about 1 μm thick and the flux of the plasma jet is 21 MW/m^2 during the torch passage at one location. The coating obtained is presented in Fig. 20. It comprises (Fig. 20a) a columnar structure (about 5 μm thick) on the side of the stainless steel substrate followed by a granular structure (see Fig. 20b). The 5 μm corresponds to a good heat withdrawal through the stainless steel substrate. However, once zirconia thickness has reached these 5 μm , heat withdrawal is drastically reduced. According to the plasma heat flux, the next deposited layers may remain in a melted state.

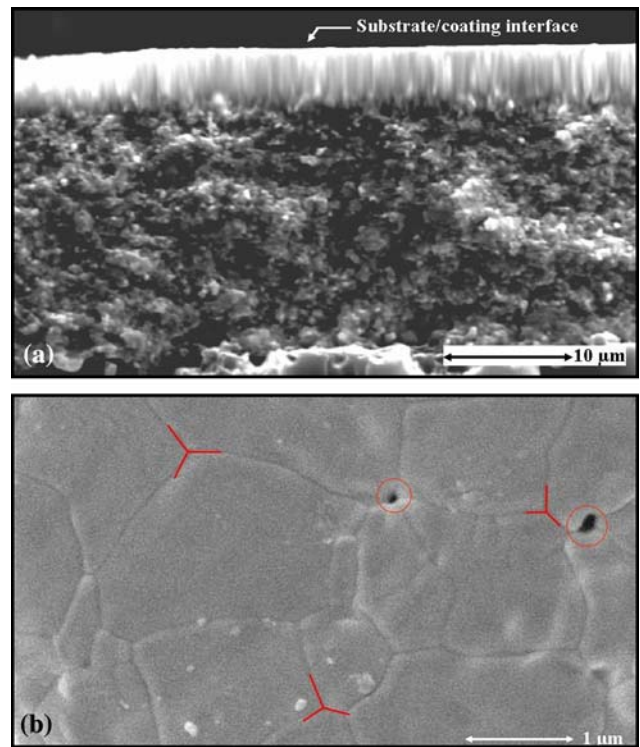


Fig. 20 Zirconia suspension plasma sprayed (Ar-H_2) onto a stainless steel substrate and detached from its substrate. (a) Fractured cross section and (b) detail of the polished cross section obtained after heat treatment (heated to 1400 $^\circ\text{C}$ at 25 $^\circ\text{min}$, isothermal treatment during 6 min and cooled down in the furnace) to reveal grain boundaries

To interpret this result, one-dimensional thermal model can be used. It consists in evaluating the perfect contact temperature, or interface temperature, T_i , between a 1- μm -thick zirconia melted pass (T_d) and a zirconia substrate (T_s). The interface temperature T_i is obtained for semi-infinite media. If heat is not yet propagated within materials, that is, $t \ll L_d^2/\alpha_d$ ($t \ll 1.6 \mu\text{s}$), where L_d is the pass thickness (m) and α_d its thermal diffusivity (m^2/s) of deposited zirconia melted pass, T_i is given by the following expression:

$$T_i = \frac{b_s T_s + b_d T_d}{b_s + b_d} \quad (\text{Eq 12})$$

b_s and b_d being respectively the effusivity of the zirconia substrate and that of melted zirconia pass.

Figure 21 represents the dependence of the interface temperature T_i on the zirconia substrate temperature T_s . It is assumed that homogenous nucleation will occur if the last deposited layer is kept fully melted, over nucleation temperature T_n (it is supposed that $T_n = 0.75 \times T_M$, where T_M is the melting temperature). Figure 21 shows that, as soon as $T_s > 1100$ $^\circ\text{C}$, conditions are fulfilled to achieve a granular nucleation. Of course, on the stainless steel substrate where T_s is lower, columnar structure is obtained and they last over a thickness of about 5 μm , that is, five passes. It has to be noted that the variation of the sub-

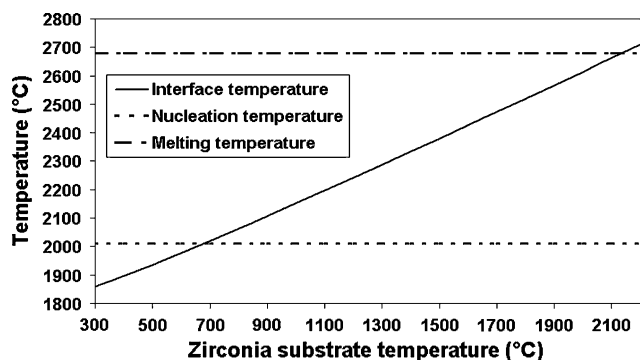


Fig. 21 Calculated evolution (1D model) of the interface temperature between two successive zirconia passes


strate temperature T_s as depicted in Fig. 21 is plausible because the amplitude of substrate temperature ΔT depends upon the heat flux q_w , the exposition duration δt (a few milliseconds) and material properties following. Considering indeed again, the approximation of semi-infinite materials, ΔT is as follows:

$$\Delta T = \frac{2q_w}{b_s} \sqrt{\frac{\delta t}{\pi}} \quad (\text{Eq 13})$$

The exposition duration, δt , is linked to the relative speed of the plasma torch and the substrate. Consequently, considering stainless steel substrate or zirconia one, ΔT can vary from 100 °C up to 2000 °C during each pass due to different material properties.

4.3.2 Solution Spraying of Zirconia. When spraying the solution precursor of aqueous acetate and nitrate salts of zirconium and yttrium, as described in Sect. 4.1.3, unpyrolyzed precursors are trapped in the successive passes as confirmed by TGA and DTA analysis (Ref 65). Coatings produced contain uniformly vertical cracks which improve their resistance to thermal cycling (Ref 49, 84, 86) compared to APS and even EBPVD coatings. After a careful study of the stress generated during coating formation (expansion mismatch and cooling stress), Xie et al. (Ref 60) have concluded that these cracks were formed by the unpyrolyzed precursor's decomposition and crystallization. This occurs during their deposition or post-deposition heat treatment at temperatures of 700 °C (precursor deposition occurs at 350 °C) provided the heating rate is over 20 °C/min due to kinetics of the reactions. The phenomena are accompanied by large volume shrinkage which can be as large as 2-3% resulting in in-plane tensile stress, sufficient to create vertical cracks.

Gell et al. (Ref 49) have schematically divided the plasma jet in three entrainment regions: I cold periphery, II moderate temperature regions (close to the jet core), and III hot inner core. The chemical and physical processes that a droplet undergoes are strongly dependent on the heating it experiences. Thus part of droplets treated in regions II, and some of them in region I, will be incorporated in the central part of the bead resulting mainly from droplets treated in the hot region III, and most of them will create the more powdery bead wings. This is



observed in each single bead, or more easily in overlapped beads (Ref 50) at the same position, their central part being denser than their wings. The same scenario is valid for suspension spraying. It is clear that limiting particle fragmentation in the jet fringes will diminish the inclusion of unmelted or poorly treated particles in each bead and between successive passes.

5. Coating Morphologies

As it can be inferred from the preceding phenomena, coating morphologies will be strongly linked to drops fragmentation and droplets penetration within the plasma jet.

5.1 Suspension Coatings

When the first bead, which has roughly a Gaussian shape (Ref 50), is deposited, its central part is well adherent and relatively dense while its wings are mostly powdery and not very adherent. One powdery wing is then covered over by the next bead. If in conventional spraying the next bead is generally sprayed at a distance equal to half of its width at half maximum height, in liquid spraying this distance is smaller (e.g., one tenth of its width). With such overlapping, the powdery wings are covered by the material coming from the hotter regions of the plasma and the dense part of the preceding bead by the material coming from colder regions of the plasma and so on. Thus each adherent pass of the coating is a mixture of the coating material from both the hot and cold regions. However, part of the powdery material, when spray conditions are suitably adjusted, is partly blown out during spraying. Moreover, the presence of vaporized materials from the hot regions, recondensing at the surface of the substrate or coating under formation, will contribute to defects within each pass. At last, the high heat flux problem must be taken into account because small ceramic particles (<1 μm) have the tendency to stick the coating surface over 700-800 °C (Ref 87). Thus, when spraying the next pass, the tiny no-melted particles, which have traveled in the jet fringes, or those vaporized in the jet core and then re-condensed will also stick in front of the successive beads and create defects between two successive passes.

The influence of the particle morphologies and size distributions will be illustrated together with the choice of the plasma forming gas adapted to particles to be treated. The different yttria (8 mol%) stabilized zirconia particles used are summarized in Table 1. They were all sprayed with either Ar-H₂ or Ar-He plasmas at the same spray distance (Ref 88).

First of all, when using nanosized particles which have the tendency to agglomerate and aggregate, such as the Tosoh TZ-8Y, resulting in a broad particle size distribution between 0.1 and 4 μm, the coating is very porous as illustrated in Fig. 22(a). Of course, this result was obtained after optimizing the suspension and its mechanical injection conditions. Figure 22(b) shows that porosities contain

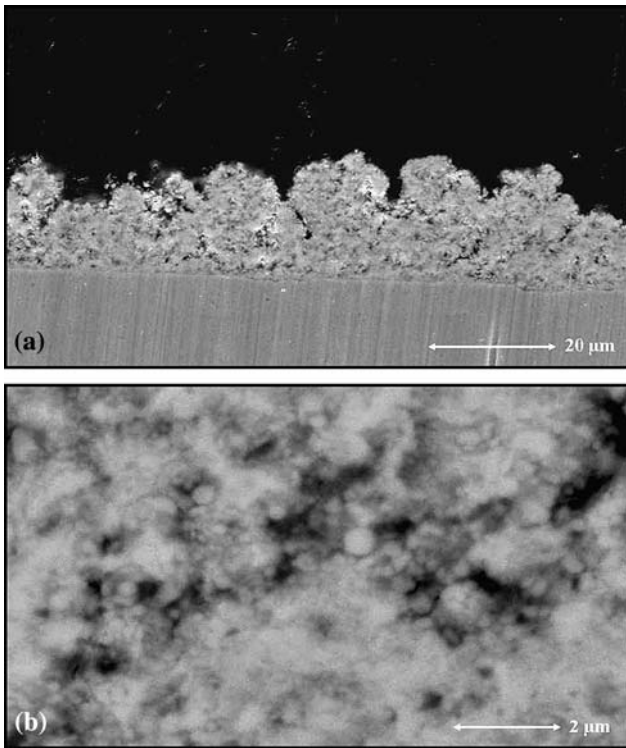


Fig. 22 (a) YSZ coating obtained with a suspension with 7 wt.% of Tosoh Z-8Y powder (Table 1) in ethanol injected in Ar-H₂ (45-15 slm) plasma jet where the enthalpy is 17.9 MJ/kg and anode nozzle 6 mm in i.d. (b) Detail of the coating

many tiny particles, almost spherical, in the range 0.05-0.3 μm. These tiny particles are evaporated and are then recondensed on the coating during its formation creating defects. The agglomerates fragmentation creates a large dispersion of trajectories and nonuniform treatments of particles resulting in coatings with poor cohesion. When spraying, with the same spray conditions, attrition-milled particles (0.15-3 μm), the coating is denser and less porous (~6%) (see Fig. 23).

The Marion powder, made of nanosized grains (20-40 nm), presents much less agglomerates, and especially aggregates, than the Tosoh powder and its size distribution is between 0.03 and 0.9 μm. When it is sprayed with an Ar-He plasma with the same enthalpy as that of the Ar-H₂ plasma used to spray the Tosoh powder, the results are quite different as illustrated in Fig. 24. The coating is rather dense (porosity of 4.5%) and its morphology is close to that of the coating obtained with attrition-milled pow-

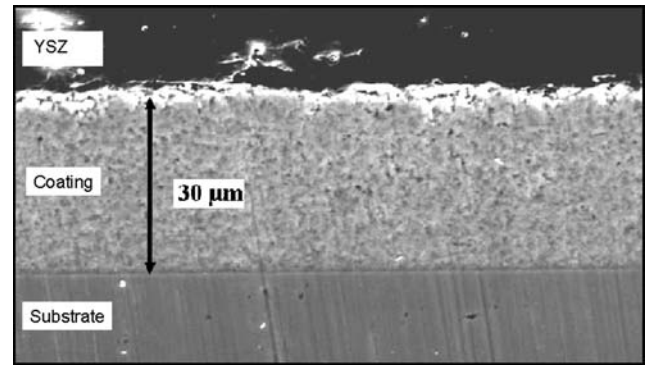


Fig. 23 YSZ coating obtained with a suspension with 7 wt.% of attrition-milled Z-8Y powder (Table 1) in ethanol injected in Ar-H₂ (45-15 slm) plasma jet where the enthalpy is 17.9 MJ/kg and anode nozzle 6 mm in i.d.

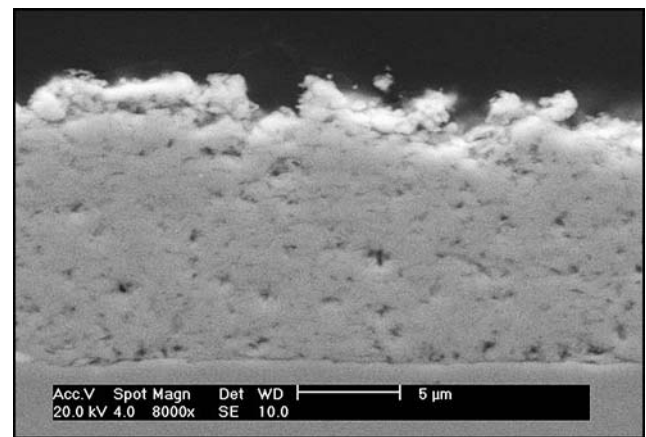


Fig. 24 YSZ coating obtained with a suspension with 20 wt.% of Marion powder (nanograins) (Table 1) in ethanol injected in Ar-He (30-30 slm) plasma jet where the enthalpy is 17.9 MJ/kg and anode nozzle 6 mm in i.d.

der (see Fig. 23). This is due to the much less voltage fluctuation with Ar-He ($\Delta V/V = 0.25$ against 1 for Ar-H₂) and the lower heat transfer coefficient of this mixture. Besides, the heat flux imposed to the substrate and coating at the same spray distance was 17.9 MW/m² instead of 20 MW/m² for the Ar-H₂ plasma. When using a powder (UC.001h) with size distribution similar to that of the nano-powder Marion but attrition milled, as shown in Fig. 25, slightly denser coatings are obtained (porosity 4%). Similar results are obtained when bigger particles, again attrition milled, are used.

Table 1 Powders used in suspensions

Powder name	$d_{0.1}^*$, μm	$d_{0.5}^*$, μm	$d_{0.9}^*$, μm	Mean grain size, nm	Wt.% of powder in suspension
Tosoh-TZ-8Y	0.10	1.5	3.5	30	7
Medipur attrition-milled	0.15	1	3	>150	7
Marion	0.03	0.06	0.76	20-40	20
UC-001h attrition-milled	0.03	0.05	0.29	30	20
UC-002h attrition-milled	0.26	0.39	0.7	260	20

* By number

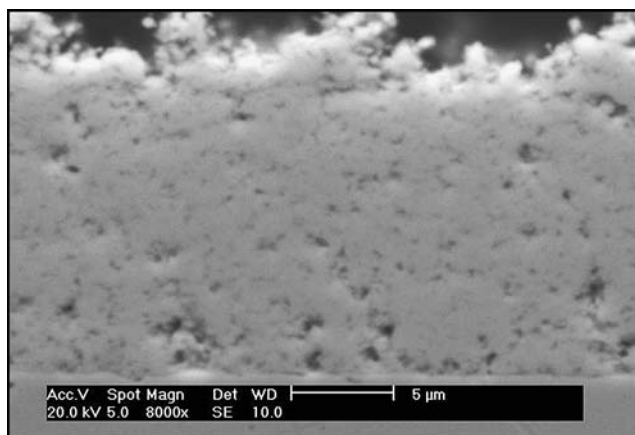


Fig. 25 YSZ coating obtained with a suspension with 20 wt.% of UC-001 attrition-milled powder (Table 1) in ethanol injected in Ar-He (30-30 slm) plasma jet where the enthalpy is 17.4 MJ/kg and an anode nozzle 6 mm in i.d

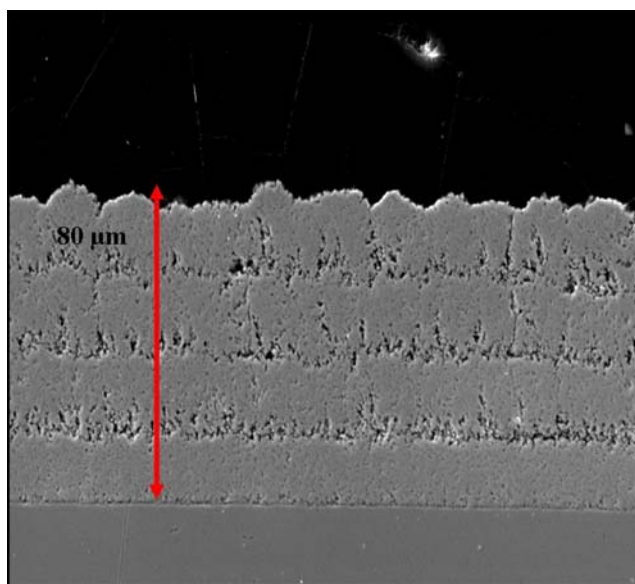


Fig. 26 Cross section of four passes deposited in conditions of Fig. 24 caption but with UC 002h (Table 1)

It has been already observed that unmelted tiny particles have strong tendency to stick to hot ($T > 1000$ °C) zirconia layers. When injecting many particles (suspension with 20 wt.% of solid particles) at the end of each pass when starting to spray the next one, particles traveling in jet fringes stick on the previously deposited and still very hot pass. This is illustrated in Fig. 26. During pass deposition with x - y pattern with beads overlapping of 1/20, the phenomenon also occurs but the tiny particles are included within beads and do not perturb the coating cohesion. However, between each pass, beads are deposited on unmelted tiny particle coming from jet fringes and sticking at the hot pass surface. Figure 26 shows the deposition of four successive passes with the defects created between them by this deposition of unmelted tiny

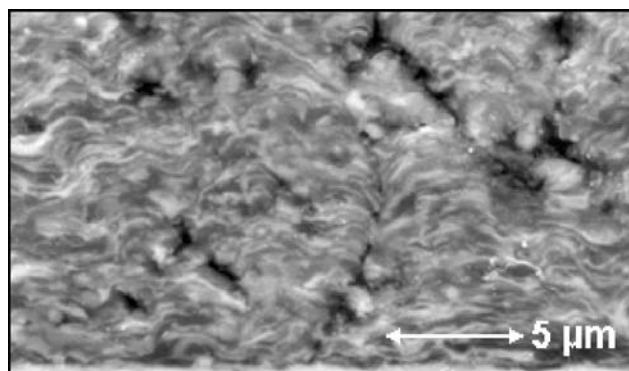


Fig. 27 Cross section of an alumina-YSZ coating obtained with suspension spraying with the spray conditions of Fig. 22 caption, but with a torch nozzle i.d. of 5 mm instead of 6 mm

particles. It is also important to note that on the cold stainless steel substrate only few unmelted particles have been deposited and the first pass is dense even close to the substrate. It is no more the case for the new successive passes which are more porous close to the previously deposited one. This phenomenon can be avoided by changing the spray pattern and the suspension mass load.

When considering dense coatings such as those of Fig. 23-25 it has not been possible to observe their structure probably due to the absence of contrast between two YSZ splats and the good contact between them. Thus alumina-YSZ mixed injection has been achieved in order to control the microstructure obtained with this process. YSZ powder was the Tosoh with a specific surface area of $13 \text{ m}^2/\text{g}$, while alumina powder (Baikowski™ CR125) had a specific area of $105 \text{ m}^2/\text{g}$. They were mixed with the same weight and the suspension solvent was ethanol and the spray parameters where those of Tosoh (see Fig. 22 caption) except that the nozzle i.d. was 5 mm to increase the plasma jet velocity (Ref 86). Figure 27 shows that the structure of the coating is made up of YSZ and alumina splats alternatively layered (there is a difference of contrast between both oxides: grey for alumina and white for YSZ) with thickness lower than 100 nm, as observed on splat by AFM. Moreover, it could be noticed that, except the porosity, the contact between splats seems to be excellent. Similar results were obtained by Oberste-Berghaus et al. (Ref 35).

5.2 Solution Coatings

Gell et al. (Ref 89) underline that the YSZ coating obtained by solution spraying comprises dense area, unmelted particles, porosity and through thickness vertical cracks produced, as seen in Sect. 4.4.2 by pyrolysis of the unmelted precursors trapped in the coating. Jordan et al. (Ref 84) explain that porous regions in such coatings are maximized by retaining more of the unpyrolyzed precursor that arrives off the centerline of the torch. They underline that an important parameter to control this porosity is, once the solution injection parameters have been optimized (Ref 50), the spray pattern. "Small inter-pass raster scan step height is both most efficient in retaining the

low-density deposits off the centerline and provides more passes at a given location for the accumulation of low density deposits compared with a large step height" (Ref 84). When making TBCs it is desirable to have semi-pyrolized material embedded within coating because they are critical for the formation of vertical cracks (Ref 49).

As already mentioned, using an injector with a very narrow atomized jet and drops in the size range 1-20 μm , dense coatings (more than 97%) of YSZ (7 wt.%) were obtained as well as eutectic alumina-zirconia (YSZ 7 wt.%) coatings with density higher than 98% and a hardness of 1117 HV under a load of 0.98 N (Ref 55).

5.3 Coating Adhesion

In conventional thermal spray, coating adhesion is mainly mechanical which means that the substrate roughness has to be adapted to the splat mean diameter. The height of surface peaks must be about one-third to one half of the mean splat diameter (Ref 90). Moreover, adhesion is increased by a factor more than 2 if the substrate is preheated over the so-called transition temperature (Ref 61). For example, with YSZ sprayed onto 316L stainless steel substrate, the coating adhesion reaches 60 MPa, against 25 MPa, when the substrate is preheated over 250 $^{\circ}\text{C}$. This preheating induces adsorbates and condensates evaporation and the formation of a nanoscale roughness with a positive skewness ($SK \sim 1$).

The questions that arise here are the following: Which roughness must have the substrate for a good adhesion of splats with diameters generally below 1 μm ? Does the transition temperature play the same role as in conventional plasma spraying? A partial answer to the last question has already been given for the elements initiating coating: splats (see Sect. 2.3.3) and illustrated in Fig. 3. Tests have been made in Limoges to spray YSZ coatings on stainless steel substrates with an Ra of 0.1 μm corresponding to Rt of 0.8 μm , height adapted to splats where the diameter was between 0.5 and 4 μm (see Fig. 14). On cold 316L substrate, the adhesion was rather poor with coating delaminating partly at the end of spray process. On preheated ones (over 250 $^{\circ}\text{C}$), adhesion values reached 20 ± 3 MPa. This value is rather close to that obtained by Gell et al. (Ref 49) with grit blasted surface (a priori obtained, according to the paper of Xie et al. (Ref 50), with alumina grit which mesh size was #320). It is also worth noting that with suspensions of fine (below 80 nm) alumina and zirconia particles, mild steel substrates were grit blasted with 60 grit alumina particles (Ref 91). To conclude this part, too few systematic experiments on the adhesion of these finely structured coatings have been performed to give a definite answer to this adhesion problem.

6. Example of Results

Of course, these liquid spraying techniques are still at their infancy: almost two decades for RF spraying and about one for dc spraying but many promising results have

already been obtained. Most of the works were devoted to SOFC's electrolyte and electrodes, thermal barriers, photo-catalytic titanium di-oxide, hydroxyapatite, WC-Co, complex oxides and metastable phases, functional materials.

6.1 SOFC's Components

With dc plasmas, advantage of the high heat flux of the plasma jet at short spray distances was taken to achieve fully dense zirconia coatings (see Fig. 20) with a granular structure. Suspensions were sprayed onto ceramic layers to form the electrolyte of SOFCs (Ref 21, 22). To achieve a better ionic conductivity at lower temperature gadolinium- or samarium-doped ceria (SDC) can be used. SDC nanoparticles (<20 nm) put in suspension have been sprayed by Bouachira et al. (Ref 27) using a PT F4 torch or a Mettech III (axial injection) one. Dense coatings were obtained with no crack, provided the substrate expansion coefficient was close to that of the deposit.

Using RF plasma tentative was made to realize CeO_2 double-doped electrolytes for lowering the SOFC's working temperature. Ceria electrolytes with various compositions and dopant concentrations were synthesized with a combinatorial chemistry approach. For that solution plasma spraying was used with nitrate salts (Ref 92).

The most commonly used anode materials for solid oxide fuel cells (SOFCs) are Ni-YSZ cermets which have both catalytic properties for hydrogen oxidation and good electronic conductivity (Ref 92, 93). A major disadvantage of such anodes is a low tolerance to sulfur and carbon deposition due to the nickel when using hydrocarbon fuels. A promising nickel-free anode to work with methane as fuel is a perovskite-type compound: $\text{La}_{0.75}\text{Sr}_{0.25}\text{Cr}_{0.5}\text{Mn}_{0.5}\text{O}_3$ (LSCM) (Ref 93, 94). By doping it with noble metal such as iridium, ruthenium, or rhodium, the electronic conductivity, the chemical stability, and the catalytic behavior are clearly improved. Sub-micronic powders of LSCM (perovskite) were dispersed in an aqueous rhodium nitrate solution before being sprayed in energetic plasma. The particle population presented a majority of fine particles, which had a diameter around 100 nm, and some bigger ones. In the suspension, the fine particles agglomerated, resulting in sizes lower than 1 μm (Ref 95). The size of the particles forming the skeleton of the coating corresponds to the granulometry of the feeding suspension. This indicates the conservation of the initial structure (Fig. 28). The analysis of the catalyst distribution reveals a uniform inclusion of rhodium in the coating with an average concentration of 0.1% in accordance with specifications.

Spraying the cathode is not necessarily very easy because LaMnO_3 doped with SrO, CaO... is prone to decompose easily over the melting temperature. This has been illustrated by the work of Monterubio et al. (Ref 96) who have shown that pure LaMnO_3 (the easiest to decompose) can be sprayed with <10% of La_2O_3 formation if particles are doped with 10 mol% of MnO_2 , with sizes between 1 and 5 μm (mean size 3 μm) and sprayed with pure Ar dc plasma jet to limit, as much as possible the

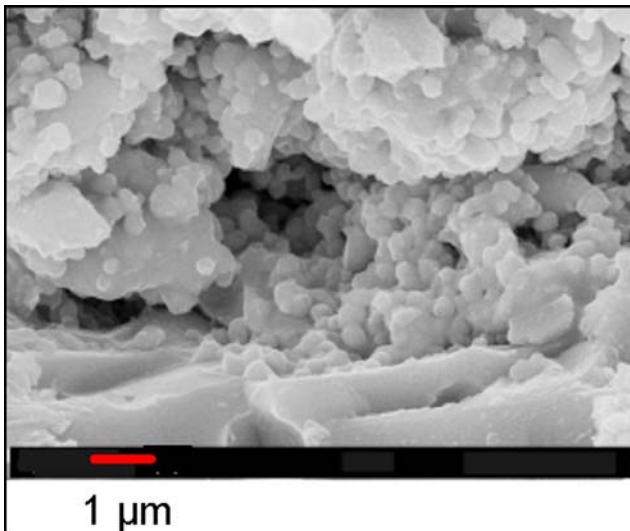
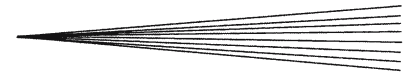


Fig. 28 Nanostructured coating of $\text{La}_{0.75}\text{Sr}_{0.25}\text{Cr}_{0.5}\text{Mn}_{0.5}\text{O}_x$ obtained by suspension plasma spraying (Ref 95)

heat transfer. Of course, perovskite doped with SrO are much easier to spray with more than 96% of them keeping their initial structure. Suspension spraying of cathodes made of $\text{La}_{0.65}\text{Sr}_{0.3}\text{MnO}_3$ and YSZ has also been studied by Kassner et al. (Ref 30) (for more details see the paper in this issue). LaMnO_2 cathodes were also sprayed with RF plasmas by Schiller et al. (Ref 43) using a suspension of MnO_2 in a saturated ethanol LaCl_3 solution. The phase purity of the perovskite coatings was further improved by post-treatment with 80% oxygen plasma. In principle, the homogeneity of the perovskite phase could be substantially improved by using precursors with lower lanthanum content but a completely single-phase, large area perovskite coating could at first not be achieved (Ref 97). It was therefore concluded that the volatility of MnO is not the only reason for the limited purity of the perovskite phase. Since La_2O_3 shows by far the highest melting point of the simple oxides of the different considered elements, it was assumed that clusters of La_2O_3 might form in the hot zone along the plasma jet by homogeneous nucleation. These clusters are then deposited onto the substrate in addition to the perovskite phase which is usually formed by heterogeneous nucleation. A breakthrough concerning phase purity was achieved when using precursors where La was substituted by Pr. With the slightly non-stoichiometric composition $\text{Pr}_{0.58}\text{Sr}_{0.4}\text{Co}_{0.2}\text{Fe}_{0.8}\text{O}_3$ (PSCF) absolutely pure perovskite phase was detected by XRD over the whole deposited layer area (Ref 97).

6.2 Thermal Barriers Coatings

YSZ coatings were sprayed using Tosoh powder and also Treibasher AG nano powder ($d_{50}=25$ nm against 300 nm for Tosoh powder) in ethanol suspension and using either Triplex I or Triplex II plasma guns (Ref 30). They show segmentation cracks: about 7 mm (for more details see the paper in this issue) which is probably due to rather thick pass with a strong temperature gradient, if the

phenomenon is the same as in conventional spraying (Ref 95, 98). To our knowledge, this is the only TBC sprayed by suspension plasma spraying.

Many works have been devoted to TBCs using solution plasma spraying (SPPS) (Ref 49, 50, 69, 84, 86, 88) by the Department of Metallurgy and Materials Engineering of the University of Connecticut. With this technique, they obtained TBCs which are even more durable than the state-of-art of EB-PVS TBCs (Ref 89). The zirconia coatings obtained have a medium thermal conductivity ($1.0\text{--}1.2$ W/m K^{-1} against about 0.8 W/m K^{-1} for APS coatings but $1.5\text{--}2.0$ W/m K^{-1} for EB-PVD ones (Ref 69)), 3D micrometer and nanometer pores, through thickness vertical cracks: about 7 mm, ultra fine splats and inter-pass boundaries (Ref 49). Of course, when comparing the lifetime of TBCs, it is the whole system that is involved: zirconia coatings, bond coat, and substrate as underlined by Gell et al. (Ref 89). Probably, on the same substrate and bond coat, deposited SPPS and EB-PVD TBCs would have the similar durability. However, the former is potentially less expensive to produce and has a lower thermal conductivity. For more details, see Gell et al. (Ref 49) in this issue.

6.3 Titania Coatings

They are mostly used for their photo catalytic properties which seem to depend mainly on their crystalline structure and the first works on the topic with conventional plasma sprayed coatings were those of Ohmori et al. (Ref 99). As underlined by Toma et al. (Ref 66), it is generally assumed that the metastable phase, anatase, presents higher photo-catalytic activity than the stable one, rutile. However, some anatase powders containing small quantities of rutile have a better photo-catalytic efficiency than that of pure anatase. The advantage of plasma sprayed suspensions lies in the surface morphologies obtained, the possibility to keep maximum anatase content and better decomposition of pollutants due to the reduced size of particles (Ref 66). Of course, it means that the spray conditions must be adapted to have a sufficient quantity of melted particles to build the coating. Good results (only anatase was detected within coatings) have been obtained for the destruction of NO (36–38%) and NO_x (15%) when spraying a water suspension (25 wt.% of powder) of 82 vol.% anatase (25 nm) and 18 vol.% rutile (50 nm) (Ref 100). With ethanol as solvent, the heat transfer is improved (less cooling of the plasma than water) and anatase content decreases drastically.

When starting from rutile TiO_2 , with a larger diameter than previously (0.33 μm) with water as solvent, the 2^3 full factorial plan performed by Jaworski et al. (Ref 101) showed that mostly the spray distance has a significant influence on the anatase fraction in coatings. This was attributed to the increase of the number of particles solidified in flight.

RF plasma was also used to spray an aqueous suspension of (V, Nb, and Ta) doped TiO_2 and the spray parameters adjusted to obtain as much as possible anatase (Ref 41). Key parameters were the injection of surplus oxygen into the plasma jet and adjusting powder carrier gas flow rate. In

spite of the rather low anatase content of coatings, the presence of titania multiphase heterostructures, acting as coupled semi-conductors systems, appears to enhance the photo catalytic effect. At last the interest of suspension plasma sprayed titania as large-area or large-scale field emitter has been demonstrated (Ref 102).

6.4 Hydroxyapatite (HA)

Bio-ceramics based on calcium phosphate compounds are currently used for various biomedical applications. However, thick coatings of HA dc plasma sprayed are often partially decomposed and contaminated with electrode materials. On the contrary, RF plasmas allow melting relatively large particles in an oxidizing atmosphere. As early as in 1996, a colloidal suspension was brought into the RF discharge core via a gas atomizing probe (Ref 44, 51), drops containing needles of HA were flash dried, melted, and then deposited. The decomposition of HA was minimized by using moderate enthalpy and a high oxidizing reactor (Ref 40, 44). As when spraying materials prone to decompose such as perovskite, the operating windows are rather narrow.

6.5 WC-Co

The potential of suspension plasma spraying for consolidation of nanostructured WC-Co coatings has been explored by Oberste-Berghaus et al. (Ref 24). Suspensions of ethanol or mixtures of ethanol and ethylene-glycol (25%) were prepared with either soft-agglomerated powders with a nominal carbide grain size of 60-250 nm or agglomerated and sintered powders with a carbide grain size of 40-80 nm. They were sprayed with Mettech Axial III torch which working conditions were for example: 275 slm, Ar 75 vol.%, N₂ 10 vol.%, H₂ 15 vol.%, 200 A, 90.1 kW. Porosity of coatings was as low as <0.2% when particle velocities were increased over 700 m/s. However, it was not possible to avoid the degradation and oxidation of carbide phase because temperatures of particles below 2200 °C could not be produced and the best hardness achieved was below 800 HV_{0.3} (against 1000-1500 HV_{0.3} for conventional coatings and nanostructured ones sprayed by HVOF with micrometric particles made of agglomerated nanoparticles). However, it must be underlined that these are very preliminary results.

6.6 Complex Oxides and Metastable Phases

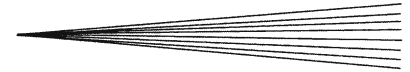
Nano composites of alumina-zirconia can potentially exhibit higher hardness, fracture toughness, slower crack growth, and lower thermal conductivity than alumina or zirconia alone (Ref 91). Using the Mettech Axial III plasma torch, suspensions of alumina-zirconia powders were sprayed. Two different initial size distributions were used: respectively <80 nm, called NA, but resulting in a size distribution of agglomerates and aggregates in suspension between 1.5 and 20 μm, and slightly larger nanoparticles, called SF, with a bi-modal suspension size distribution between 0.1 and 5 μm. The constituents

Al₂O₃-ZrO₂-Y₂O₃ were different in weight ratios: NA respectively 57-42-1 and SF 60-40-0 and phase content (percentages of monoclinic, m, for zirconia and, α phase for alumina). Spray conditions, according to particle velocities (up to almost 700 m/s for NA) and temperatures (between 2750 and 2950 °C) lowered the percentages of m and α and resulted in rather dense coatings ($P < 1.9\%$) with a fine lamellar structure of alternating zirconia and alumina layers (similar to that of Fig. 27). Particles collected in flight have distributions similar to those of the particles within the suspension. One of the coatings with NA powder exhibits a high hardness (1125 HV_{0.3}) with a good abrasion resistance. For more details about those promising results see (Ref 91).

Al₂O₃-ZrO₂ and Al₂O₃-ZrO₂-Y₂O₃ systems were studied by Vasiliev et al. (Ref 70, 71) using the solution spraying with 3 MB plasma torch. The precursors were aqueous solution of zirconium and aluminum salts. When starting with pure zirconia, coatings were, as expected, in monoclinic phase. With 10 mol% Al₂O₃-90 mol% ZrO₂ coatings, about 75% dense, consisted of nanostructures primarily with t-ZrO₂ phase with a chemical composition of Zr/Al = 83/17 (atomic ratio). Al³⁺, otherwise insoluble in ZrO₂ under equilibrium conditions, is in solid solution with ZrO₂ leading to the partial stabilization of t-ZrO₂. With the ternary mixtures (mol%) 10Al₂O₃-86.4ZrO₂-3.6Y₂O₃ (10AlZrY) and 20Al₂O₃-76.4ZrO₂-3.6Y₂O₃ (20AlZrY) nanostructures in coatings are primarily t-ZrO₂ and c-ZrO₂ with no Al₂O₃ phase in these nanostructured regions. Al³⁺, in addition to Y³⁺, is in solid solution with ZrO₂ leading to stabilization of its t and c phases.

6.7 Functional Materials

Using RF plasmas, Ravi et al. (Ref 39, 103) have studied solution/sol spraying to develop functional oxides from precursors. They studied Eu-Y₂O₃ luminescent coatings, Yttrium Aluminum Garnet (YAG) and Yttrium Iron Garnet (YIG). They succeeded in depositing dense nanostructures in few tens of seconds using TAFA and TEKNA PL-100 torches fed with about 200 mL of sol. They showed that the Eu-Y₂O₃ coating presented a uniform distribution of Eu³⁺ among 0.5-5 μm particles where Eu and Y were both present (Ref 39). Plasma spraying of hybrid sol (mixture of bohemite and yttrium nitrate in water) or citrate-nitrate solution (mixture of yttrium nitrate, aluminum nitrate, and citric acid in water) irrespective of the high degree of homogeneity resulted into kinetically stable crystalline phases (Ref 103). On the other hand, regular and reverse co-precipitate sols resulted in amorphous coatings which transformed into single phase YAG upon heat treatment (Ref 103). YIG precursor sol (regular and reverse) were prepared (Ref 39) and resulted in an amorphous deposit transformed in a nanostructured coating upon annealing (800-1000 °C). Lanthanum strontium manganite coatings were also obtained to study the possibility to use them for magnetic sensor applications. Of course, many works are still necessary to optimize such coatings but these works open a



very interesting route to explore the chemistry field of complex oxides.

7. Conclusions

Coating technology, especially plasma spraying, combining synthesis and consolidation processes into a single operation allows spraying nanostructured or at least finely structured materials in one operation. Coatings being achieved by layering fully melted particles, nanostructured coatings can be obtained by injecting particles whose size is sub-micrometric or nanometric. Since about more than one decade, many works have been devoted to spraying oxides starting from sub-micron particles. According to the low mass of such particles, the carrier gas of conventionally sprayed particles has to be replaced by a liquid (solution, sol, or suspension). However, liquid injection by either atomization (drops) or mechanical injection (jet or drops) is complex and the diameter and velocity v_ℓ of liquid injected have to be controlled. This is especially the case for radial injection in dc plasma jets, where drops or jet momentum density $\rho_\ell v_\ell^2$ must be higher than that of the plasma ρv^2 varying drastically along its radius and axis. According to the brightness of plasma jets, the radial injection can only be monitored by using laser flashes and CCD cameras. Two types of plasma torches can be used, RF and dc. The main difference between both is the plasma velocity and the possibility to achieve an oxidizing atmosphere with RF plasmas. With dc plasma jets (with radial and axial injection) according to liquid/plasma relative velocities, u , easily over 1000 m/s, fragmentation of drops or jets occurs within times at least two orders of magnitude lower than drops vaporization. On the contrary, with RF plasmas, no fragmentation occurs. One of the problems of drops or jet radial injection with dc plasma jets is that fragmentation starts in the jet fringes entraining resulting droplets in rather low temperature zones. It results, for suspensions in unmelted or partially melted particles and for solutions in partially pyrolyzed ones. The surface tension σ_ℓ of the solvent also plays an important role in drops fragmentation; however, if a higher σ_ℓ (e.g., water versus ethanol) delays fragmentation in the jet fringes, it usually consumes more plasma energy to be vaporized. The fast fragmentation of drops and droplets together with solvent vaporization, followed by its dissociation and ionization, cools very rapidly dc plasma jets inducing spray distances much shorter than in conventional spraying (40-50 mm against 100-120 mm). With dc torches the injection problem is made more difficult by arc root fluctuations at the anode. Resulting power fluctuations ΔP relatively to the mean power dissipated, \bar{P} , can be with conventional torches as high as $\Delta P/\bar{P} > 1$ with plasma forming gases containing diatomic gases against $\Delta P/P < 0.3$ for monatomic gases, while with Triplex guns working only with Ar-He $\Delta P/P < 0.1$. These fluctuations are almost linearly followed by the plasma flow velocity v . It thus results in more drastic variations of the plasma momentum density and consequently drops fragmentation. Once fragmentation is achieved, suspension

or solution droplets do not behave the same way upon solvent vaporization.

With suspension, the solid particles contained in each droplet are released and their behavior within the plasma jet strongly depends on their ability to agglomerate or aggregate. The behavior of agglomerates or aggregates is not necessarily predictable because they can explode upon solvent evaporation or keep their size. As the size of solid particles must be adapted to the plasma heat transfer, explosion of “big” particles may result in tiny particles which can be vaporized and create defects upon recondensation on the coating under formation, especially if its temperature is over 700-800 °C. Fine particles (below about 0.3 μm) are prone to follow the flow and, if their Stokes number at the flow boundary layer close to the substrate is below one, they will never impact it. Thus, velocities must be as high as possible for small particles. This is achieved, according to AccuraSpray ensemble measurements, by using Mettech Axial III torch (up to 700 m/s). High velocities can also be achieved by HVOF spraying where liquid is injected instead of particles (Ref 91, 104). However, if slightly higher velocities (compared to those obtained with Mettech Axial III torch) can be achieved, the particle heating is not necessarily sufficient for good inter-splat adhesion. With RF plasmas, once the solvent of big drops has been evaporated, solid particles of suspensions are flash sintered, melted, reacted, and sprayed as micrometric drops (tens of micrometers) as in conventional spraying. This route allows synthesizing and spraying oxides very sensitive to decomposition such as hydroxyapatite or perovskite.

The phenomena are quite different with solutions. With dc plasma jets, the precipitation will form a more or less porous shell of precipitate. The precipitate formation depends on droplets sizes and solute initial mass fraction. To simplify, droplets below 5 μm will result in solid particles then melted, while larger particles fragment and produce, especially for those traveling in jet fringes, deposition of un-pyrolyzed particles. If, in Solution Precursor Plasma Spraying, what happens to droplets in dc plasma torches has been studied in detail, it is not the case, to our knowledge, of solution drops in RF plasmas, where only coatings have been characterized. Compared to suspension, the main interest of solutions is the possibility to develop new chemistry because of the molecular level mixing of constituents. Sol spraying also seems to be very promising; however, only very few papers have been published and the way solid particles in flight and coating are formed is not yet explained.

Coatings, as with conventional spraying, are made by overlapping beads. Of course, according to the way solutions or suspensions are deposited, each bead thickness is rather in the few micrometers thickness instead of the few tens in conventional spraying. The central part of the bead, corresponding to particles that have been treated in the plasma jet core (at least when using radial injection with dc torches) are generally rather dense and made of layered splats where the diameter is between 0.1 and few micrometers and thicknesses between 50 and 150 nm. On the contrary, their wings are more porous, even powdery

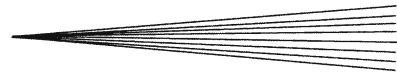
and result mainly from particles whose trajectories were in the jet core fringes resulting in partially melted particles or un-pyrolized precipitates from solutions. Thus, according to the spray patterns controlling beads overlapping, a more or less important part of these partially treated materials will be included within each pass. For zirconia they will result in porous coatings (with suspensions) or vertically cracked thermal barriers with solutions. The latter results from the pyrolysis of precipitates, creating an important volume variation ($\sim 3\%$), when heated by the plasma torch. It is thus important to underline the necessity of a good control both of liquid injection and spray pattern. Another problem that differentiates such coatings from conventional ones is the spray distance where heat fluxes for a PTF4 torch are between 10 and 21 MW/m² instead of about 2 MW/m² in conventional spraying. It results in strong thermal gradients within YSZ coatings, even if their thickness is a few micrometers, implying using a substrate not too different in expansion coefficient to avoid cracks formation. However, such heat fluxes, well controlled, bring some advantages such as in situ coating densification, which for zirconia coatings can result in a granular structure for suspensions and pyrolysis of un-pyrolized materials for solutions resulting in vertical cracks. On the other hand, the high surface temperature of each pass unfortunately favor sticking of small un-melted particles or recondensed vaporized ones creating defects between two successive passes, if care is not taken to limit as much as possible the formation of these small particles.

At last, it must be emphasized that interesting applications of these techniques, still in their infancy, have been developed for SOFC's components, thermal barrier coatings with a resistance to thermal cycling equivalent to that of EB-PVD deposited ones, very intricate coatings of alumina and zirconia with better mechanical properties than zirconia, metastable phases alumina-zirconia, titanium oxide for photo-catalytic applications, functional coatings (YAG, YIG,...).

Of course much, work is still necessary before industrial applications are developed using nanostructured coatings achieved by suspension or solution plasma spraying. Other routes may also show up such as Vacuum Cold Spraying (Ref 105).

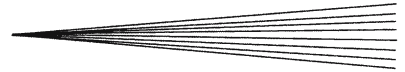
References

- J.J. Karthikeyan, C.C. Berndt, S. Reddy, J.-Y. Wang, A.H. King, and H. Herman, Nanomaterial Deposits Formed by dc Plasma Spraying of Liquid Feedstocks, *J. Am. Ceram. Soc.*, 1998, **81**(1), p 121-128
- P. Angerer, L.G. Yu, K.A. Khor, G. Korb, and I. Zalite, Spark-Plasma-Sintering (SPS) of Nanostructured Titanium Carbonitride Powders, *J. Eur. Ceram. Soc.*, 2005, **25**, p 1919-1927
- M. Gell, E.H. Jordan, Y.H. Sohn, D. Goberman, L. Shaw, and T.D. Xiao, Development and Implementation of Plasma Sprayed Nanostructured Ceramic Coatings, *Surf. Coat. Technol.*, 2001, **146-147**, p 48-54
- R.S. Lima, A. Kucuk, and C.C. Berndt, Bimodal Distribution of Mechanical Properties of Plasma Sprayed Nanostructured Partially Stabilized Zirconia, *Mater. Sci. Eng. A*, 2002, **327**, p 224-232
- H. Chen, Y. Zhang, and C. Ding, Tribological Properties of Nanostructured Zirconia Coatings Deposited by Plasma Spraying, *Wear*, 2002, **253**, p 885-893
- H. Chen and C.X. Ding, Nanostructured Zirconia Coating Prepared by Atmospheric Plasma Spraying, *Surf. Coat. Technol.*, 2002, **150**, p 31-36
- H. Chen, X. Zhang, and C. Ding, Investigation of the Thermo Mechanical Properties of Plasma-sprayed Nanostructured Zirconia Coating, *J. Eur. Ceram. Soc.*, 2003, **23**, p 1449-1455
- B. Liang and C. Ding, Phase Composition of Nanostructured Zirconia Coatings Deposited by Air Plasma Spraying, *Surf. Coat. Technol.*, 2005, **191**, p 267-273
- O. Racek, C.C. Berndt, D.N. Guru, and J. Heberlein, Nanostructured and Conventional YSZ Coatings Deposited Using APS and TTPR Techniques, *Surf. Coat. Technol.*, 2006, **201**, p 338-346
- R.S. Lima and B. Marple, Thermal Spray Coatings Engineered from Nanostructured Ceramic Agglomerated Powders for Structural, Thermal Barrier and Biomedical Applications, *J. Therm. Spray Technol.*, 2007, **16**(1), p 40-63
- J. Karthikeyan, C.C. Berndt, J. Tikkanen, S. Reddy, and H. Herman, Plasma Spray Synthesis of Nanomaterial Powders and Deposits, *Surf. Coat. Technol.*, 1997, **238**(2), p 275-286
- E. Bouyer, F. Gitzhofer, and M. Boulos, Parametric Study of Suspension Plasma Sprayed Hydroxyapatite, *ITSC 1996*, C.C. Berndt, Ed. (Materials Park, OH, USA), ASM International, 1996, p 683-691
- F. Gitzhofer, E. Bouyer, and M.I. Boulos, Suspension Plasma Spray Deposition, US Patent no 5602921, 1997
- L. Jia and F. Gitzhofer, Inductively Coupled Thermal Plasma Synthesis of Cerium Oxide Nano-Powders, *Conferences International sur la Projection Thermique de Suspension 2007*, Eds. (CEA Le Ripault), cd-rom
- N.P. Padture, K.W. Schlichting, T. Bhatia, A. Ozturk, B. Cetegen, E.H. Jordan, M. Gell, S. Jiang, T.D. Xiao, P.R. Strutt, E. Garcia, P. Mirazano, and M.I. Osendi, Towards Durable Thermal Barrier Coatings with Novel Microstructures Deposited by Solution-precursor Plasma Spray, *Acta Mater.*, 2001, **49**, p 2251-2257
- L. Xie, X. Ma, E.H. Jordan, N.P. Padture, T.D. Xiao, and M. Gell, Identification of Coating Deposition Mechanisms in Solution Precursor Plasma-spray Process Using Model Spray Experiments, *Mater. Sci. Eng. A*, 2003, **362**, p 204-212
- E.H. Jordan, L. Xie, C. Ma, M. Gell, N. Padture, B. Cetegen, J. Roth, T.D. Xiao, and P.E.C. Bryant, Superior Thermal Barrier Coatings Using Solution Precursor Plasma Spray, *J. Therm. Spray Technol.*, 2004, **13**(1), p 57-65
- X. Ma, F. Wa, J. Roth, M. Gell, and E.H. Jordan, Low Thermal Conductivity Thermal Barrier Coating Deposited by the Solution Plasma Spray Process, *Surf. Coat. Technol.*, 2006, **201**, p 4447-4452
- P. Fauchais, V. Rat, C. Delbos, J.F. Coudert, T. Chartier, and L. Bianchi, Understanding of Suspension dc Plasma Spraying of Finely Structured Coating for SOFC, *IEEE Trans. Plasma Sci.*, 2005, **33**(2), p 920-930
- J. Fazilleau, C. Delbos, V. Rat, J.F. Coudert, P. Fauchais, and B. Pateyron, Phenomena Involved in Suspension Plasma Spraying, Part 1: Suspension Injection and Behavior, *Plasma Chem. Plasma Process.*, 2006, **26**(4), p 371-391
- C. Delbos, J. Fazilleau, V. Rat, J.F. Coudert, P. Fauchais, and B. Pateyron, Phenomena Involved in Suspension Plasma Spraying Part 2: Zirconia Particle Treatment and Coating Formation, *Plasma Chem. Plasma Process.*, 2006, **26**(4), p 393-414
- P. Fauchais, R. Etchart-Salas, C. Delbos, M. Tognovi, V. Rat, J.F. Coudert, and T. Chartier, Suspension and Solution Plasma Spraying of Finely Structured Coatings, *J. Phys. D: Appl. Phys.*, 2007, **40**, p 2394-2406
- F.L. Toma, G. Bertrand, D. Klein, C. Coddet, and C. Meunier, Nanostructured Photocatalytic Titania Coatings Formed by Suspension Plasma Spraying, *J. Therm. Spray Technol.*, 2006, **15**(4), p 587-592
- J. Oberste-Berghaus, B. Marple, and C. Moreau, Suspension Plasma Spraying of Nanostructured WC-12Co Coatings, *J. Therm. Spray Technol.*, 2006, **15**(4), p 676-681
- S. Basu, E.H. Jordan, and B.M. Cetegen, Fluid Mechanisms and Heat Transfer of Liquid Precursor Droplets Injected into High Temperature Plasmas, *J. Therm. Spray Technol.*, to be published in this issue doi:10.1007/s11666-007-9140-6



26. X.Q. Ma, T.D. Xiao, J. Roth, L.D. Xie, E.H. Jordan, N.P. Padture, M. Gell, X.Q. Chen, and J.G. Price, Thick Thermal Barrier Coatings with Controlled Microstructure Using Solution Precursor Plasma Spray Process, *Thermal Spray 2004, Advances in Technology and Application* (Materials Park, OH, USA), ASM International, 2004, p 1103-1109
27. S. Bouaricha, J. Oberste-Berghaus, J.-G. Legoux, C. Moreau, and D. Ghosh, Production of Samarium Doped-ceria Plasma Sprayed Nano-coatings Using an Internal Injection of a Suspension Containing Nanoparticles, *ITSC 2005* (Düsseldorf, Germany), DVS, 2005, e-proceedings
28. J. Oberste-Berghaus, J.-G. Legoux, and C. Moreau, Injection Conditions and In-flight Particle States in Suspension Plasma Spraying of Alumina and Zirconia Nano-ceramics, *ITSC 2005* (Düsseldorf, Germany), DVS, 2005, e-proceedings
29. R. Siegert, J.-E. Doring, J.-L. Marqués, R. Vassen, D. Sebold, and D. Stöver, Denser Ceramic Coatings Obtained by the Optimization of the Suspension Plasma Spraying Technique, *ITSC 2004* (Düsseldorf, Germany), DVS, 2004, e-proceedings
30. H. Kassner, R. Siegert, D. Hathiramani, R. Vassen, and D. Stöver, Application of the Suspension Plasma Spraying (SPS) for the Manufacture of Ceramic Coatings, *J. Therm. Spray Technol.*, to be published in this issue doi:[10.1007/s11666-007-9144-2](https://doi.org/10.1007/s11666-007-9144-2)
31. M.P. Planche, J.F. Coudert, and P. Fauchais, Velocity Measurements for Arc Jets Produced by d.c. Plasma Spray Torches, *Plasma Chem. Plasma Process.*, 1998, **18**, p 263-283
32. P. Roumilhac, J.F. Coudert, and P. Fauchais, Influence of the Arc Chamber Design and the Surrounding Atmosphere on the Characteristics and Temperature Distributions of Ar-H₂ and Ar-He Spraying Plasma Jets, *Plasma Proc. and Synthesis of Materials*, D. Apelian and J. Szekely, Eds. (Pittsburg, PN, USA), MRS, 1990, **190**, p 227-242
33. H.-Me Höle and G. Barbezat, Triplex II-A Quantum Leap in Plasma Spraying, *Proc. of 48 Int. Wissenschaftliches Kolloquium*, Tech. Univ. Ilmenau, Germany, Session 7, Plasma Processing, 2003, e-proceedings
34. Fr.-W. Bach, D.K. Möhwald, and D. Kolar, Qualification of a Modified Triplex II Plasma Gun for Processing of Liquid Precursors and Wire or Powder Shaped Spray Materials under Controlled Atmosphere, *ITSC 2005* (Dusseldörf, Germany), DVS, e-proceedings
35. J. Oberste-Berghaus, S. Boccaricha, J.G. Legoux, C. Moreau, and T. Chraska, Suspension Plasma Spraying of Nanoceramics Using an Axial Injection Torch, *ITSC 2005* (Dusseldörf, Germany), DVS, e-proceedings
36. G. Matthäus, The Tri-electrode Axial Injection Plasma Torch "Axial III"-Equipment and Coating Application, *Proc. of 48 Int. Wissenschaftliches Kolloquium* Tech. Univ. Ilmenau, Germany, Session 7, Plasma Processing, 2003, e-proceedings
37. C. Moreau, P. Gougeon, A. Burgess, and D. Ross, Characterization of Particle Flows in Axial Injection Plasma Torch, *Thermal Spray: Science and Technology*, C.C. Berndt and S. Sampath, Eds. (Materials Park, OH, USA), ASM International, 1995, p 141-147
38. J.G. Legoux, B. Aesenault, C. Moreau, V. Bouyer, and L. Leblanc, Evaluation of Four High Velocity Thermal Spray Guns Using WC-10Co-4Cr Cermets, *Thermal Spray: Surface Engineering via Applied Research*, C.C. Berndt, Ed. (Materials Park, OH, USA), ASM International, 2000, p 479-486
39. B.G. Ravi, S. Sampath, R. Gambino, P.S. Devi, and J.B. Parise, Plasma Spray Synthesis from Precursors: Progress, Issues and Considerations, *J. Therm. Spray Technol.*, 2006, **15**(4), p 701-707
40. R. Kumar, P. Cheang, and K.A. Khor, RF Plasma Processing of Ultra Fine Hydroxyapatite Powders, *Surf. Coat. Technol.*, 2001, **113**(1-3), p 456-462
41. I. Burlacov, J. Jirkovsky, M. Müller, and R.B. Heimann, Induction Plasma Sprayed Photo Catalytically Active Titania Coatings and their Characterization by Micro-Raman Spectroscopy, *Surf. Coat. Technol.*, 2006, **201**(1-2), p 255-264
42. G. Schiller, M. Müller, F. Gitzhofer, M.I. Boulos, and R.B. Heimann, Suspension Plasma Spraying (SPS) of Cobalt Spinel, *Thermal Spray: A United Forum for Scientific and Technological Advances*, C.C Berndt, Ed. (Materials Park, OH, USA), ASM International, 1997, p 343-347
43. G. Schiller, M. Müller, and F. Gitzhofer, Suspension Plasma Spraying for the Preparation of Perovskite Powders and Coatings, *Thermal Spray: A United Forum for Scientific and Technological Advances*, C.C Berndt, Ed. (Materials Park, OH, USA), ASM International, 1997, p 349-352
44. F. Gitzhofer, Suspension Plasma Spraying by Induction Thermal Plasma Technology, *J. Therm. Spray Technol.*, accepted
45. M.I. Boulos, The Inductively Coupled Radio-frequency Plasma, *J. High Temp. Mater. Process.*, 1997, **1**, p 17-36
46. J. Lu and F. Gitzhofer, Preparation of Nanostructured Dense and Thin Electrolyte for SOFCs by Suspension Plasma Spraying, presented at ITSC2007, Beijing, May 2007
47. F.L. Toma, G. Bertrand, R. Rampon, D. Klein, and C. Coddet, Relationship between the Suspension Properties and Liquid Plasma Sprayed Coating Characteristics, *ITSC 2006* (Materials Park, OH, USA), ASM International, 2006, e-proceedings
48. R. Rampon, G. Bertrand, F.L. Toma, and C. Coddet, Liquid Plasma Sprayed Coatings of Yttria stabilized for SOFC Electrolyte, *ITSC 2006* (Materials Park, OH, USA), ASM International, 2006, e-proceedings
49. M. Gell, E.H. Jordan, M. Teicholz, B.M. Cetegen, N. Padture, L. Xie, D. Chen, X. Ma, and J. Roth, Thermal Barrier Coatings made by the Solution Precursor Plasma Spray Process, *J. Therm. Spray Technol.*, doi:[10.1007/s11666-007-9141-5](https://doi.org/10.1007/s11666-007-9141-5)
50. L. Xie, X. Ma, A. Ozturk, E.H. Jordan, N.P. Padture, B.M. Cetegen, D.T. Xiao, and M. Gell, Processing Parameter Effects on Solution Precursor Plasma Spray Process Spray Patterns, *Surf. Coat. Technol.*, 2004, **183**(1), p 51-61
51. E. Bouyer, F. Gitzhofer, and M. Boulos, Parametric Study of Suspension Plasma Sprayed Hydroxyapatite, *Thermal Spray: Practical Solutions for Engineering Problems*, C.C. Berndt, Ed. (Materials Park, OH, USA), ASM International, 1996, p 683-691
52. I. Filkova and P. Cedik, Nozzle Atomization in Spray Drying, *Advances Drying*, A.S. Mujumdar, Ed., Hemisphere Pub. Corp., 1984, **3**, p 181-215
53. P. Rampon, C. Filiatre, and G. Bertrand, Suspension Plasma Spraying of YPSZ Coatings for SOFC: Suspension Atomization and Injection, *J. Therm. Spray Technol.*, doi:[10.1007/s-11666-007-9143-3](https://doi.org/10.1007/s-11666-007-9143-3)
54. A.H. Lefebvre, *Atomizations and Sprays*, Hemisphere Pub. Corp., 1989
55. E.H. Jordan, M. Gell, P. Bonzani, D. Chen, S. Basu, B. Cetegen, F. Wu, and X. Ma, Making Dense Coatings with the Solution Precursor Plasma Spray Process, *Thermal Spray 2007: Global Coating Solution*, B.R. Marple, M.M. Hyland, Y.-C. Lau, C.-J. Li, R.S. Lima, and G. Montavon, Eds. (Materials Park, OH, USA), ASM International, 2007, p 463-470, e-proceedings
56. K. Wittmann, J. Fazilleau, J.F. Coudert, P. Fauchais, and F. Blein, A New Process to Deposit Thin Coatings by Injecting Nanoparticles Suspensions in a d.c. Plasma Jet, *ITSC 2002*, E. Lugsheider, Ed. (Düsseldorf, Germany), DVS, 2002, p 519-522
57. C. Delbos, J. Fazilleau, J.F. Coudert, P. Fauchais, L. Bianchi, and K. Wittmann-Ténéze, Plasma Spray Elaboration of Fine Nanostructured YSZ Coatings by Liquid Suspension Injection, *Thermal Spray: Advancing the Science and Applying the Technology*, B.R. Marple and C. Moreau, Eds. (Materials Park, OH, USA), ASM International, 2003
58. K. Wittmann, F. Blein, J. Fazilleau, J.F. Coudert, and P. Fauchais, A New Process to Deposit Thin Coatings by Injecting Nanoparticles Suspensions in a d.c. Plasma Jet, *ITSC 2002*, E. Lugsheider, Ed. (Düsseldorf, Germany), DVS, 2002, e-proceedings
59. R. Siegert, J.E. Doring, J.L. Marqués, R. Vassen, D. Sebold, and D. Stöver, Influence of Injection Parameters on the Suspension Plasma Spraying Coating Properties, *ITSC 2005*, E. Lugsheider, Ed. (Düsseldorf, Germany), DVS, 2002, e-proceedings
60. P. Blazdell and S. Kuroda, Plasma Spraying of Submicron Ceramic Suspensions Using a Continuous Ink Jet Printer, *Surf. Coat. Technol.*, 2000, **123**(2-3), p 239-246
61. J. Cedelle, M. Vardelle, and P. Fauchais, Influence of Stainless Steel Substrate Preheating on Surface Topography and on Mil-

- limeter and Micrometer-sized Splat Formation, *Surf. Coat. Technol.*, 2006, **201**(3-4), p 1378-1382
62. L. Bianchi, A. Denoirjean, F. Blein, and P. Fauchais, Microstructural Investigation of Plasma Sprayed Ceramic Splats, *Thin Solid Films*, 1997, **299**, p 125-135
 63. J.F. Bisson, M. Lamontagne, and C. Moreau, Ensemble In-flight Particle Diagnostics under Thermal Spray Conditions, *Thermal Spray 2001: New Surfaces for New Millennium*, C. Berndt, K.A. Khor, and E.F. Lugsheider, Eds. (Materials Park, OH, USA), ASM International, 2001, p 705-714
 64. J. Fazilleau, C. Delbos, M. Violier, J.F. Coudert, P. Fauchais, L. Bianchi, and K. Wittmann-Ténèze, Influence of Substrate Temperature on Formation of Micrometric Splats Obtained by Plasma Spraying Liquid Suspension, *ITSC 2003*, B.R. Marple and C. Moreau, Eds. (Materials Park, OH, USA), ASM International, 2003, p 889-895
 65. L. Xie, D. Chen, E.H. Jordan, A. Ozturk, F. Wa, X. Ma, B.M. Cetegen, and M. Gell, Formation of Vertical Cracks in Solution-precursor Plasma Sprayed Thermal Barrier Coatings, *Surf. Coat. Technol.*, 2006, **201**(3-4), p 1058-1064
 66. F.L. Toma, D. Sokolov, G. Bertrand, D. Klein, C. Coddet, and C. Meunier, Comparison of the Photocatalytic Behavior of TiO₂ Coatings Elaborated by Different Thermal Spray Processes, *J. Therm. Spray Technol.*, 2006, **15**(4), p 576-581
 67. FR0453390, Revêtement nanostructuré et procédé de revêtement, CEA Le Ripault, Monts, 37, France (in French)
 68. Ph. Prené, L. Beurain Montouillout, K. Vallé, and Ph. Belleville, The CEA Sol-gel Technology for Coatings, *4th International Conference on Coatings on Glass*, Brauchweig (Allemagne), 2002, Proceedings 167-173
 69. A.D. Jadhav, N.P. Padture, E.H. Jordan, M. Gell, P. Miranzo, and E.R. Fullu, Low Thermal Conductivity Plasma Sprayed Thermal Barrier Coatings with Engineered Microstructure, *Acta Mater.*, 2006, **54**(12), p 3343-3349
 70. A.L. Vasiliev, N.P. Padture, and X. Ma, Coatings of Metastable Ceramics Deposited by Solution Precursor Plasma Spray: I-Binary ZrO₃-Al₂O₃ System, *Acta Mater.*, 2006, **54**(19), p 4913-4920
 71. A.L. Vasiliev, N.P. Padture, and X. Ma, Coatings of Metastable Ceramics Deposited by Solution Precursor Plasma Spray: II-Ternary ZrO₃-Y₂O₃-AlO₃ System, *Acta Mater.*, 2006, **54**(19), p 4913-4920
 72. Y.P. Chyow and E. Pfender, Behavior of Particles in Thermal Plasma Flows, *Plasma Chem. Plasma Proc.*, 1989, **9**, p 45-71
 73. S.S. Hwang, Z. Liu, and R.D. Reitz, Break-up Mechanisms and Drag Coefficients of High Speed Vaporizing Liquid Drops, *Atomization Sprays*, 1996, **6**, p 353-376
 74. B.E. Gelfand, Droplet Break-up Phenomena in Flows with Velocity Lag, *Prog. Energy Combust. Sci.*, 1996, **22**, p 201-265
 75. T. Watunabe and K. Ebihara, Numerical Simulation of Coalescence and Break-up of Rising Droplets, *Comput. Fluids*, 2003, **32**, p 823-834
 76. A. Ozturk and M. Cetegen, Modeling of Plasma Assisted Formation of Precipitates in Zirconia Containing Liquid Precursor Droplets, *Mater. Sci. Eng. A*, 2004, **384**, p 331-351
 77. A. Ozturk and M. Cetegen, Experiments on Ceramic Formation from Liquid Precursor Spray Axially Injected into an Oxy-acetylene Flame, *Acta Mater.*, 2005, **53**, p 5203-5211
 78. S. Basu, E.H. Jordan, and B.M. Cetegen, Fluid Mechanics and Heat Transfer of Liquid Precursor Droplets Injected into High Temperature Plasmas, *J. Therm. Spray Technol.*, 2006, **15**(4), p 576-581
 79. M.I. Boulos, P. Fauchais, A. Vardelle, and E. Pfender, Fundamentals of Plasma Particle Momentum and Heat Transfer, *Plasma Spraying: Theory and Applications*, S. Suryanarayanan, Ed. (Singapore), World Scientific, 1993
 80. G.I. Taylor, The Shape and Acceleration of a Drop in a High Speed Air Stream, Technical Report, in the Scientific Papers of G.I. Taylor, Ed., G.K. Batchelor, 1963
 81. C. Marchand, C. Chazelas, G. Mariaux, and A. Vardelle, Liquid Precursor Plasma Spraying: Modelling the Interaction between the Transient Plasma Jet and the Droplets, to be published in ITSC 2007 Proceedings
 82. P. Fauchais, J. Fazilleau, C. Delbos, J.F. Coudert, L. Bianchi, K. Wittmann-Ténèze, and A. Denoirjean, Studies of Micrometric Splats Obtained by Suspension d.c. Plasma Spraying, *Proc. of ISPC16*, R. d'Agostino, Ed. (Italy), Univ. of Bari, e-proceedings
 83. C. Delbos, J. Fazilleau, V. Rat, J.F. Coudert, P. Fauchais, and L. Bianchi, Influence of Powder Size Distribution and Heat Flux on Yttria Stabilized Zirconia Coatings Elaborated by Suspension Injection in a d.c. Plasma Jet, *ITSC 2005* (Düsseldorf, Germany), DVS, 2005, e-proceedings
 84. E.H. Jordan, L. Xie, X. Ma, M. Gell, N.P. Padture, B. Cetegen, A. Ozturk, J. Roth, T.D. Xiao, and P.E.C. Bryant, Superior Thermal Barrier Coatings Using Solution Precursor Plasma Spray, *J. Therm. Spray Technol.*, 2004, **13**(1), p 57-65
 85. A. Ozturk and B. Cetegen, Modeling of Axially and Transversely Injected Precursor Droplets into a Plasma Environment, *Int. J. Heat Mass Transfer*, 2005, **48**(21-22), p 4367-4383
 86. L. Xie, X. Ma, E.H. Jordan, N.P. Padture, D.T. Xiao, and M. Gell, Deposition Mechanisms of Thermal Spray Barrier Coatings in the Solution Precursors Plasma Spray Process, *Surf. Coat. Technol.*, 2004, **177-178**, p 103-107
 87. A. Haddadi, R. Hamacha, A. Grimaud, P. Fauchais, and F. Nardou, Residual Stresses and Microstructure of Plasma Sprayed Zirconia Coatings, *High Temp. Mater. Processes*, 1998, **2**(3), p 327-337
 88. C. Delbos, J. Fazilleau, V. Rat, J.F. Coudert, P. Fauchais, and L. Bianchi, Finely Structured Ceramic Coatings Elaborated by Liquid Suspension Injection in d.c. Plasma Jets, *ITSC 2004 Proc.* (Dusseldorf, Germany), DVS, e-proceedings
 89. M. Gell, L. Xie, E.H. Jordan, and N.P. Padture, Mechanisms of Spallation of Solution Precursor Plasma Spray Thermal Barrier Coatings, *Surf. Coat. Technol.*, 2004, **188-189**, p 101-106
 90. P. Fauchais, Understanding Plasma Spraying – An Invited Review, *J. Phys. D: Appl. Phys.*, 2004, **37**, p R1-R23
 91. J. Oberste Berghaus, J.-G. Legoux, C. Moreau, F. Tarasi, and T. Chraska, Mechanical and Thermal Transport Properties of Suspension Thermal Sprayed Alumina-Zirconia Composite Coatings, *J. Therm. Spray Technol.*, doi:10.1007/s11666-007-9146-0
 92. F. Gitzhofer, M.-E. Bonneau, and M. Boulos, Double Doped Ceria Electrolyte Layer by RF Plasma Spraying, *ITSC 2001*, C.C. Berndt, K.A. Khor, and E.F. Lugsheider, Eds. (Materials Park, OH, USA), ASM International, 2001, p 61-68
 93. N.Q. Minh, Ceramic Fuel Cells, *J. Am. Ceram. Soc.*, 1993, **76**(3), p 563-588
 94. S. Tao and J.T.S. Irvine, A Redox-stable Efficient Anode for Solid Oxide Fuel Cells, *Nat. Mater.*, 2003, **2**, p 320-323
 95. K. Wittmann-Ténèze and L. Bianchi, Elaboration of an Anode for Internal Reforming by Injection of a Suspension in a d.c. Plasma, European Fuel Cell Forum, 2004, Lucerne, Switzerland
 96. C. Monterrubio-Badillo, H. Ageorges, T. Chartier, J.F. Coudert, and P. Fauchais, Preparation of LaMnO₃ Perovskite Films by Suspension Plasma Spraying for SOFC Cathode, *Surf. Coat. Technol.*, 2006, **200**, p 3743-3756
 97. G. Schiller, R. Henne, M. Lang, and M. Müller, DC and RF Plasma Processing for Fabrication of Solid Oxide Fuel Cells, *ITSC 2004* (Osaka, Japan, Düsseldorf, Germany), DVS, e-proceedings
 98. A. Tricoire, "Plasma Sprayed Thermal Barriers with Vertical Cracks: Understanding of Phenomena, Spraying and Characterization of Coatings," Ph.D. Thesis, Univ of Limoges, France Nb52-2005 (in French), 2005
 99. A. Ohmori, K.C. Park, and Y. Atara, Photoelectrochemical Properties of Plasma Sprayed TiO₂ Coatings, *Thermal Spray: Research and Applications*, T.F. Bernicki, Ed. (Materials Park, OH, USA), ASM International, 1990, p 509-515
 100. F.L. Toma, G. Bertrand, D. Klein, C. Coddet, and C. Meunier, Nanostructured Photocatalytic Titania Coatings Formed by Suspension Plasma Spraying, *J. Therm. Spray Technol.*, 2006, **15**(4), p 587-592
 101. J. Jaworski, L. Pawlowski, F. Rondet, S. Kozerski, and A.L. Magner, Influence of Suspension Plasma Spraying Process Parameter on TiO₂ Coatings Microstructure, *J. Therm. Spray Technol.*, doi:10.1007/s11666-007-9147-z



102. R. Tomaszek, Z. Znamirovski, L. Pawlowski, and A. Wojnakowski, Temperature Behavior of Titania Field Emitters by Suspension Plasma Spraying, *Surf. Coat. Technol.*, 2006, **201**(5), p 2099-2102
103. B.G. Ravi, A.S. Gandhi, X.Z. Guo, J. Margolies, and S. Sam-path, Liquid Precursor Plasma Spraying of Functional Materials: A Case Study for Yttrium Aluminium Garnet (YAG), *J. Therm. Spray Technol.*, doi:[10.1007/s11666-007-9151-3](https://doi.org/10.1007/s11666-007-9151-3)
104. A. Killinger and J. Rauch, High Velocity Suspension Flame-spraying (HVSFS), Spraying Micron and Nano-particles with Hypersonic Speed, *J. Therm. Spray Technol.*, accepted
105. S.-Q. Fan, G.-J. Yang, C.-J. Li, G.-J. Liu, C.-X. Li, and L.-Z. Zhang, Characterization of Microstructure of Nano-TiO₂ Coating Deposited by Vacuum Cold Spraying, *J. Therm. Spray Technol.*, 2006, **15**(4), p 513-517